The Astrophysical Journal Supplement Series, 151:35–73, 2004 March

INTERSTELLAR ICE: THE *INFRARED SPACE OBSERVATORY* LEGACY

E. L. Gibb[1,2]
Department of Physics, University of Notre Dame, Notre Dame, IN 46556
D. C. B. Whittet[1]
Department of Physics, Applied Physics and Astronomy, Rensselaer Polytechnic Institute, Troy, NY 12180
A. C. A. Boogert
Astronomy Department, California Institute of Technology, Pasadena, CA 91125
AND
A. G. G. M. Tielens[3]
Kapteyn Institute, P.O. Box 800, 9700 AV Groningen, Netherlands
Received 2003 August 22; accepted 2003 November 4

ABSTRACT

We present 2.5–30 μm spectra from the Short-Wavelength Spectrometer of the *Infrared Space Observatory* for a total of 23 sources. The sources include embedded young stellar objects spanning a wide range of mass and luminosity, together with field stars sampling quiescent dark clouds and the diffuse interstellar medium. Expanding on results of previous studies, we use these spectra to investigate ice composition as a function of environment. The spectra reveal an extremely rich set of absorption features attributed to simple molecules in the ices. We discuss the observed properties of these absorption features and review their assignments. Among the species securely identified are H_2O, CO, CO_2, CH_3OH, and CH_4. Likely identified species include OCS, H_2CO, and HCOOH. There is also evidence for NH_3 and OCN^- ice features, but these identifications are more controversial.

Features that continue to defy identification include the 3.3–3.7 μm "ice band wing" and the bulk of the 6.8 μm feature. In addition, we find evidence for excess absorption at 6.0 μm that cannot be attributed to H_2O ice. We examine the degree of intercorrelation of the 6.8 μm, 4.62 μm ("XCN") and 6.0 μm (excess) features. Our results are consistent with the interpretation of the 6.8 and 4.62 μm features as due to NH_4^+ and OCN^- ions, respectively, though alternative explanations cannot currently be ruled out. We find that the optical depth correlations are dependent on the profile of the 6.8 μm feature but not on the mass of the YSO nor the ice temperature along the line of sight. We discuss the implications for our current understanding of ice processing. We briefly discuss the composition, origin, and evolution of interstellar ices.

Subject headings: dust, extinction — infrared: ISM — ISM: abundances — ISM: molecules — line: profiles

1. INTRODUCTION

Dramatic progress in understanding the nature and evolution of solids in the interstellar medium has been made since the 1995 launch of the *Infrared Space Observatory* (*ISO*). The Short-Wavelength Spectrometer (SWS) instrument on-board *ISO* covered the entire 2.4–45 μm spectral range of interest for studying vibrational modes of solid state molecules, at resolving powers sufficient to extract the information contained within the profiles. Regions of the infrared spectrum not accessible from the ground because of telluric absorption were explored for the first time.

The 2.4–45 μm spectra of sources hidden at visible wavelengths by large columns of dust contain absorption features attributed to refractory solids (principally the Si—O stretching and O—Si—O bending modes of silicates at 9.7 and 18 μm, respectively), upon which are superposed absorptions of molecular ices when the line of sight intersects a dense molecular cloud (e.g., Willner et al. 1982; Whittet 2003). The dominant ice constituent is H_2O, which displays a strong O—H stretching mode at 3.05 μm together with weaker bending and combination modes at 6.0 and 4.5 μm, respectively, and a libration mode blended with the silicate features near 13 μm. Whilst H_2O appears to account for 60%–70% of the ice in most lines of sight (e.g., Whittet 2003), other species detected spectroscopically include CO, CO_2, $^{13}CO_2$, OCS, CH_3OH, CH_4, "XCN" (a C $\equiv$ N stretch possibly due to OCN^-), and possibly NH_3. There are also several features that remain largely unidentified, such as the 6.8 μm feature attributed to C-H deformation modes and/or NH_4^+. The excess absorption in the long-wavelength wing of the 3 μm water feature has also not been satisfactorily explained.

Star formation is associated with regions of dense molecular cloud material, and observations of species in the condensed phase provide insight into chemical and physical processes in such regions. Deep within these protected clouds temperatures can drop as low as 10 K. At such temperatures, atoms and molecules will collide with and stick to a grain surface, forming an ice mantle coating. Subsequently, several processes may act to modify the mantle. Atoms can thermally hop from site to site over the ice matrix or undergo quantum mechanical tunneling, eventually reacting with another atom or molecule. Water and methanol are believed to form by this

[1] New York Center for Studies on the Origins of Life, Rensselaer Polytechnic Institute, Troy, NY 12180.
[2] Department of Physics, Applied Physics and Astronomy, Rensselaer Polytechnic Institute, Troy, NY 12180.
[3] SRON, National Institute for Space Research, P.O. Box 800, 9700 AV Groningen, Netherlands.

route, adding H atoms to an O atom and CO molecule on the grain surface, respectively. Gas phase observations of molecules such as HDO indicate enhanced abundances, which cannot be explained by gas phase reactions and also indicate ice mantle modification. Close to a forming protostar, increasing temperatures and a higher flux of ultraviolet or X-ray photons lead to high-energy processing of the ice mantle and evaporation of the more volatile species. Studies of laboratory analogs have shown that energetic processing of simple ices leads to formation of more complex species such as OCN^-, NH_2CHO, and C_2H_5OH (e.g., Bernstein et al. 1995) and organic refractory matter (ORM) (Greenberg et al. 1995) spectrally similar to an acid-dissolved residue (kerogen) from Murchison and other carbonaceous meteorites (Cronin & Pizzarello 1990).

Investigating how the composition and structure of ice mantles varies as a function of physical environment is vital to understanding chemical evolution in the envelopes of young stars, protoplanetary disks, and comets. Thus far, most studies have concentrated on a single species (i.e., Gerakines et al. 1999; Whittet et al. 2001) or a single spectral feature (i.e., Chiar et al. 1995; Schutte et al. 1998), while others have concentrated on many features in a single source (i.e., van Dishoeck et al. 1998; Gibb et al. 2000). To date, no comprehensive look at the entire 2.4–45 μm spectral region in a large number of sources has been undertaken. With the *ISO* database in the public domain, such a comprehensive study is timely and much needed.

Observations and data reduction are discussed in § 2 and the laboratory fits in § 3. The nature of each source in our study is briefly reviewed in § 4. Results are discussed in § 5, and our conclusions are summarized in § 6.

2. OBSERVATIONS AND DATA REDUCTION

The data used in this paper consist primarily of complete grating scans from 2.4 to 45.2 μm in AOT mode S01 (speed 3 or 4) at a resolving power of $\sim R/4$ and $\sim R/2$, respectively (where R, the full grating resolving power of the SWS, ranges from 1000 to 2000). AOT mode S06 scans, which cover limited spectral ranges with the full resolving power of the SWS, were used when available. A detailed description of the SWS and its mode of operation is given by de Graauw et al. (1996). The observations used in this study are listed in Table 1. They were chosen by searching the *ISO* SWS database for spectra with S01 speed 3 or higher resolution exhibiting ice absorption features. The highly reddened hypergiant Cyg OB2 No.12 is also included as representative of sight lines that sample the diffuse ISM (defined here as those in which no significant ice is detected).

Data reduction was performed at the Space Research Organization of the Netherlands (SRON) in Groningen, The Netherlands, using the standard SWS interactive analysis package and pipeline processing version OLP9.0. Instrumental fringing can be a problem, particularly longward of about 8 μm. We removed fringes when necessary by using the RESP_INTER and FRINGES software routines. The *ISO* spacecraft records spectra with a grating that scans from low to high wavelengths and then from high to low wavelengths, resulting in two scans (the ''up'' and ''down'' scans). These scans were reduced separately. When flat-fielding, we made a reference flat with the down scan, which is less affected by memory effects, and applied this to the up scan. The final up and down spectra were usually found to agree well in shape and flux level and the final step was to average the two. When multiple observations in the same grating mode of a single source were available, an average was made. In cases of saturated absorption features, as occurs at both 3 and 9 μm in W33 A and AFGL 7009S, we applied a filter to the data. Points with signal-to-noise ratio of less than 3 or flux density of less than 0.1 Jy were removed (see Gibb et al. 2000 for details).

For each source, we fit a polynomial to the continuum regions and used this to derive an optical depth plot. Regions chosen to represent the continuum vary slightly from source to source to avoid emission features that are present in some lines of sight but not others. Typical regions are shortward of 2.7 μm, 4.1–4.15 μm, and 5.1–5.5 μm. To these we fit a least-χ^2 polynomial of up to fourth order. This method for determining optical depth is inadequate for extracting the 6–8 μm ice features since there are no reliable continuum points between 5.5 and 30 μm. For this reason, we used a combination of a blackbody fit through the short-wavelength side (5–5.5 μm) and a polynomial to the relatively smooth 30–45 μm region, as discussed in Keane et al. (2001c). The lack of a continuum region until longward of the 18 μm silicate feature that can be used to constrain a polynomial necessitates this approach.

Once an optical depth spectrum was derived, we calculated the column density from

$$N = \int \tau d\nu / A, \tag{1}$$

where A is the band strength (in molecules cm^{-2}) as measured in the laboratory, N is the column density in cm^{-2}, and τ is the optical depth. Table 2 lists the positions, approximate widths (FWHM), identifications, and band strengths for identified or expected vibrational modes. We note that the precise position and width for most species is a function of environment. While many *ISO* sources in this study have been the subject of previous investigations involving fits based on laboratory analogs (Chiar et al. 1998; Whittet et al. 1998; Gerakines et al. 1999; Boogert et al. 2000; Gibb et al. 2000), several others have not previously been studied in this way. In these cases, we made a least-squares fit to the feature using both apolar and polar laboratory spectra from the Leiden Molecular Astrophysics database[4] as described in Nummelin et al. (2001). For other features such as those at 3.46 and 9.75 μm that are superposed on a prominent absorption feature, we fitted a polynomial along the wing of the deeper feature to extract the weaker one as discussed in such works as Brooke, Sellgren, & Geballe (1999) and Allamandola et al. (1992). The optical depths, FWHM, and column densities derived for each species are given on a source-by-source basis in Tables 2–24.

3. FITS WITH LABORATORY ICES

Laboratories designed for studies of interstellar ice analogs have been well documented in the literature (Gerakines et al. 1995; Allamandola, Sandford, & Valero 1988; Sandford & Allamandola 1990; Hudson & Moore 1995). The absorbance spectra obtained from these investigations were used to fit the spectra of sources in our study. For several sources with high-quality spectra, we attempted to fit laboratory spectra of all known ice constituents to the optical depth plots in Figure 1. The ice mixtures used in the fits are given in Table 3.

[4] See http://www.strw.leidenuniv.nl/ ~lab.

TABLE 1

SUMMARY OF OBSERVATIONS

SOURCE	POSITION (J2000) R.A.	POSITION (J2000) Decl.	AOT	UTC DATE	t_{int} (s)	FILE
W3 IRS 5	02 25 40.5	62 05 51.3	1.3	1997 Jan 17	3434	42701302
			6	1997 Jan 17	5668	42701224
AFGL 490	03 27 38.7	58 47 01.1	1.3	1997 Aug 17	3434	64001804
			6	1997 Jul 31	6704	62301701
			6	1997 Aug 14	1872	63702402
			6	1998 Mar 27	11234	82301033
Elias 1	04 18 40.7	28 19 16.0	1.3	1997 Sep 19	3434	67301306
Elias 16	04 39 38.8	26 11 26.8	6	1997 Oct 01	8682	68600538
Orion BN	05 35 14.2	−05 22 23.6	6	1997 Oct 12	7598	69602521
Orion IRc2	05 35 14.3	−05 22 31.6	6	1997 Sep 06	7654	66002132
Mon R2 IRS 2	06 07 45.7	−06 22 50.0	1.1	1997 Oct 27	1140	71102004
Mon R2 IRS 3	06 07 47.8	−06 22 56.8	1.3	1997 Oct 27	3454	71101712
	06 07 48.2	−06 22 54.8	6	1997 Oct 27	4098	71101802
AFGL 989	06 41 10.1	09 29 35.8	1.3	1997 Oct 31	3454	72602619
AFGL 2136	11 22 26.2	−13 30 08.3	1.3	1996 Oct 11	3454	33000222
			6	1996 Mar 16	2994	12000925
			6	1996 Mar 18	1012	12200841
			6	1996 Mar 19	1244	12301305
			6	1996 Mar 24	3732	12800302
			6	1996 Sep 23	4391	31101023
			6	1997 Apr 15	6324	51601403
			6	1998 Apr 05	648	87200946
Elias 29	16 27 09.3	−24 37 21.1	1.3	1996 Aug 09	3454	26700814
			6	1995 Aug 03	5668	29200615
Sgr A*	17 45 40.0	−29 00 28.6	1.4	1996 Feb 19	6528	09401801
			6	1997 Feb 21	13114	46301102
			6	1997 Feb 21	6716	46301201
			6	1997 Feb 27	8486	46901903
			6	1997 Mar 15	1086	48401630
			6	1997 Mar 29	1808	49801104
GCS 3I	17 46 14.8	−28 49 34.0	1.3	1996 Aug 29	3454	28701246
			6	1996 Oct 08	3226	32701543
GCS 4	17 46 15.7	−28 49 47.0	1.3	1996 Sep 09	3454	29702147
W33 A	18 14 39.4	−17 52 01.4	1.4	1996 Oct 10	6538	32900920
			6	1996 Oct 14	7620	33201806
	18 14 39.0	−17 52 04.0	6	1997 Feb 25	7506	46700801
	18 14 39.4	−17 52 01.4	6	1997 Apr 17	3328	51501601
AFGL 7009S	18 34 20.6	−05 59 45.2	1.3	1996 Apr 17	3462	15201140
	18 34 20.6	−05 59 45.0	6	1996 Mar 24	10802	12800406
			6	1996 Sep 02	9559	29001801
			6	1997 Mar 02	4910	47201201
R CrA IRS 2	19 01 41.5	−36 58 28.5	1.4	1997 Apr 22	6538	52301201
	19 01 41.4	−36 58 31.0	6	1997 Mar 25	6090	49500409
R CrA IRS 1	19 01 50.7	−36 58 9.9	1.4	1997 Apr 22	6538	52301106
AFGL 2591	20 29 24.6	40 11 19.1	1.3	1996 Nov 07	3454	35700734
	20 29 24.7	40 11 19.0	6	1995 Dec 15	1972	02800582
	20 29 24.5	40 11 19.0	6	1996 Apr 07	2908	14200503
Cyg OB2 12	20 32 41.0	41 14 28.3	1.3	1997 Oct 17	3454	33504130
S140	22 19 18.2	63 18 47.6	1.4	1996 Jun 24	6538	22002135
	22 19 18.2	63 18 47.2	6	1996 Jul 06	5270	26301731
NGC 7538 IRS 1	23 13 45.3	61 28 09.9	1.1	1996 Feb 16	916	09102647
			1.3	1996 Dec 05	3454	38501842
			6	1996 Aug 25	4102	28301235
			6	1996 Dec 13	6484	38501937
NGC 7538 IRS 9	23 14 01.6	61 27 20.4	1.1	1996 Feb 28	916	09801532
			6	1996 Feb 23	6894	09801533
			6	1996 Sep 09	1802	28301334
			6	1996 Dec 11	4502	39002336
			6	1997 Jan 22	3136	43305704
			6	1997 Jun 06	3328	56801802
			6	1997 Dec 06	6264	75101049
			6	1998 Mar 16	2435	85200455

NOTE.—Units of right ascension are hours, minutes, and seconds, and units of declination are degrees, arcminutes, and arcseconds.

TABLE 2
SOME SOLID STATE TRANSITIONS OBSERVED IN THE INFRARED

Molecule	λ (μm)	$\Delta\nu$ (cm^{-1})	Vibration Mode	A (10^{-17} cm molecule^{-1})	Reference
NH_3	2.96	45	–N–H stretch	1.1	1
H_2O	3.05	335	O–H stretch	20	1, 2
$–CH_2–$, $–CH_3$	3.47	~ 10	C–H stretch	$\sim 0.1–0.4$	1
CH_3OH	3.53	30	C–H stretch	0.76	1
CH_3OH	3.95	115.3	C–H stretch	0.51	1
H_2S	3.95	45	S–H stretch	2.9	3
CO_2	4.27	18	C–O stretch	7.6	2
$^{13}CO_2$	4.38	12.9	^{13}C–O stretch	7.8	2
H_2O	4.5	700	$3\nu_L$ and/or $\nu_2 + \nu_L$	1.0	2
"XCN"	4.62	29.1	CN stretch	~ 5	4
CO	4.67	9.71	^{12}CO stretch	1.1	2
^{13}CO	4.78		^{13}CO stretch	1.3	2
OCS	4.91	19.6	C–S stretch	17	5
H_2CO	5.81	21	C=O stretch	0.96	6
HCOOH	5.85	65	C=O stretch	6.7	7
CH_3HCO	5.83		C=O stretch	1.3	7
H_2O	6.02	160	H–O–H bend	0.84	1
$HCOO^-$	6.33		C–O stretch	10	7
Organics	6.82	90	O–H bend, C-H deformation	1	1
HCOOH	7.25	16.8	C–H deformation	0.26	7
$HCOO^-$	7.25	19.8	C–O stretch	0.80	7
$HCONH_2$	7.22		C–H deformation	0.32	7
$HCOO^-$	7.41	17.8	C–O stretch	1.7	7
CH_3HCO	7.41	10.6	C–H deformation	0.15	7
SO_2	7.58	10–30	S–O (ν_3) asymmetric stretch	3.4	8
CH_4	7.70	8	C–H (ν_4) deformation	0.73	8
CH_3OH	8.9	34	C–H_3 rock	0.13	1
NH_3	9.35	68	Umbrella	1.3	9
Silicate	9.7	100	Si–O stretch		
CH_3OH	9.75	29	C–O stretch	1.8	1
H_2O	13.3	240	Libration	2.8	5
CO_2	15.3	18	O–C–O bend	1.1	2
Silicate	18		O–Si–O bend		

REFERENCES.—(1) d'Hendecourt & Allamandola 1986; (2) Gerakines et al. 1995; (3) Salama et al. 1990; (4) Schutte & Greenberg 1997; (5) Hudgins et al. 1993; (6) Schutte et al. 1993; (7) Schutte et al. 1999; (8) Boogert et al. 1997; (9) Kerkhof et al. 1999.

Laboratory fits for CO_2 are from Gerakines et al. (1999) or Nummelin et al. (2001). Those for CO are from Chiar, Adamson, & Whittet (1996). When published fits were not available, we followed the procedures outlined in these and other papers whereby least-squares fits of laboratory spectra from the Leiden Molecular Database and Hudgins et al. (1993) were made.

There are no appropriate laboratory spectra for the large number of molecules present in most sources in this paper. Most laboratory spectra are for mixtures of three or fewer components. The ice mixture is known to strongly influence the shape and position of many features, so a combination of pure ice spectra is not a reliable way to simulate a mixture. For example, the umbrella mode of pure NH_3 is at 9.3 μm but shifts to 9.0 μm when the NH_3 is a minor constituent in a polar mantle. Also, interactions of NH_3 with the H_2O-ice matrix give rise to a broad ammonium hydrate absorption near 3.5 μm. This is obviously not present when a spectrum of pure ammonia is used. Similarly, most CO_2 and CO features are consistent with two components: polar and apolar ice mixtures.

For this reason, we extracted the ice features for a specific mantle component by, for example, subtracting the water features from a water/ammonia or water/methanol mixture and scaling the resulting 2–45 μm NH_3 or CH_3OH spectrum to the appropriate optical depth for that source. Then each ice constituent is added together to build a laboratory spectrum tailored to the source in question. This is not a rigorous method of fitting a spectrum but serves the purpose of giving a general picture of the degree to which current laboratory spectra account for measured absorption features. For ices that exhibit multiple components, such as polar and apolar CO_2, the ice mixtures used are those found by fitting routines discussed by Gerakines et al. (1999), Chiar et al. (1998), Schutte et al. (1996), Palumbo, Geballe, & Tielens (1997), Gibb et al. (2000), and Gibb, Whittet, & Chiar (2001). In addition to the ices, we added an organic refractory component from Greenberg et al. (1995) to sources with excess 6 μm absorption as discussed in Gibb & Whittet (2002).

Fits of the optical depth spectra were attempted for selected sources with deep ice features and good signal-to-noise ratio. The selected sources are W33A, AFGL 7009S, Elias 29, AFGL 2136, AFGL 2591, AFGL 989, NGC 7538 IRS 9, Mon R2 IRS 3, S140, and W3 IRS 5. Results are shown in Figure 1.

4. THE SOURCES

4.1. *W3 IRS 5*

W3 IRS 5 is a doubly peaked, luminous (Ladd et al. 1993, $1.7 \times 10^5\ L_\odot$) infrared source in the W3 H II/molecular cloud

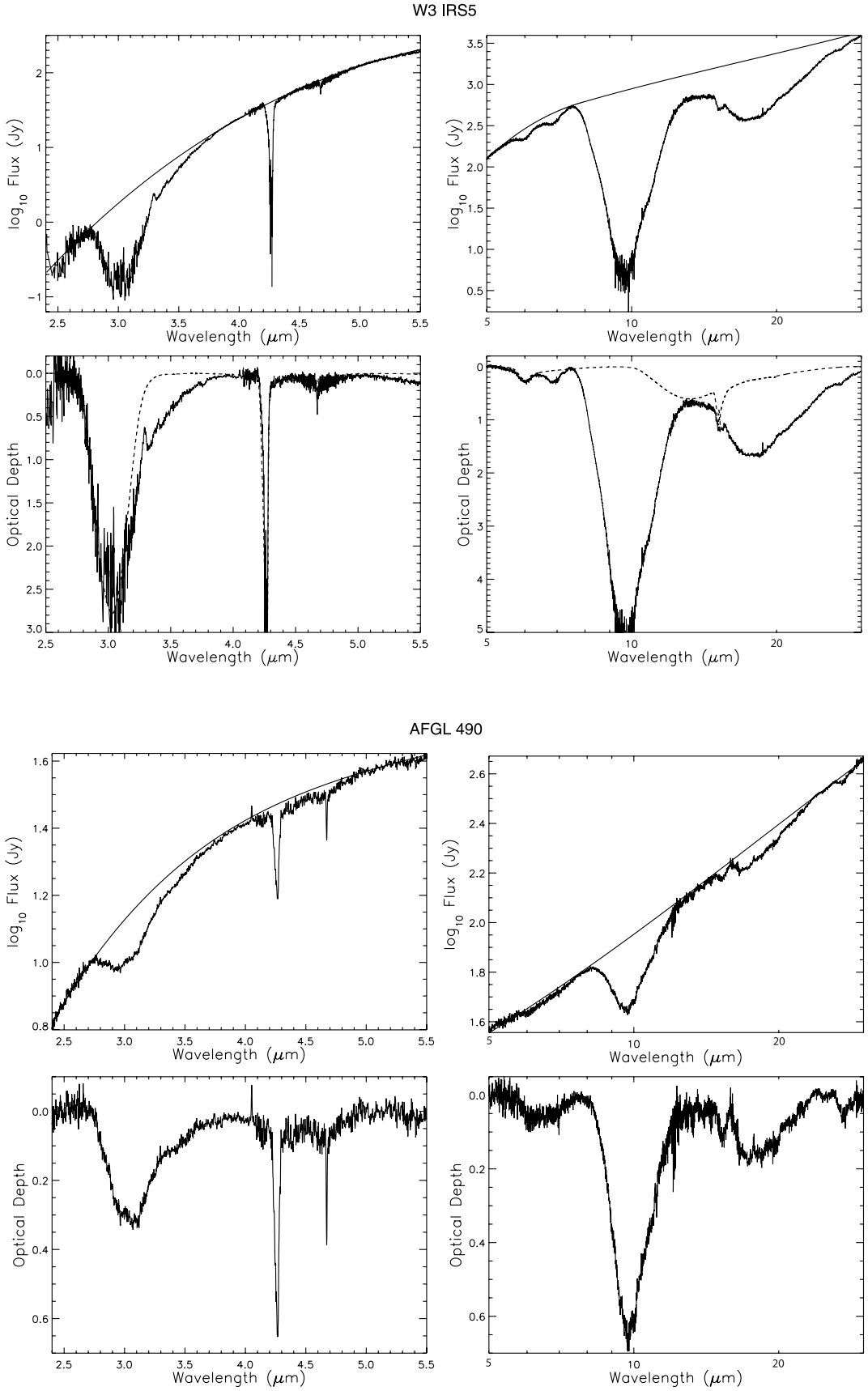

FIG. 1.—Plots of $\log_{10}$ flux (Jy) vs. wavelength (μm) with the best-fit polynomial and the corresponding optical depth plot for all the sources in this study. The left column shows the 2.4–5 μm regions, while the right shows the 5–30 μm region (the 30–45 μm region is typically a smoothly rising continuum and is left out of the plots to better exhibit the ice features). For the sources for which there is adequate signal-to-noise ratio, a composite spectrum has been fitted to all known ice components as described in § 4.1. In each case a good fit is made to the principle ice components. We note that much remains to be learned about the infrared absorbers, especially from 3.2–4 μm and 6.5–7.5 μm.

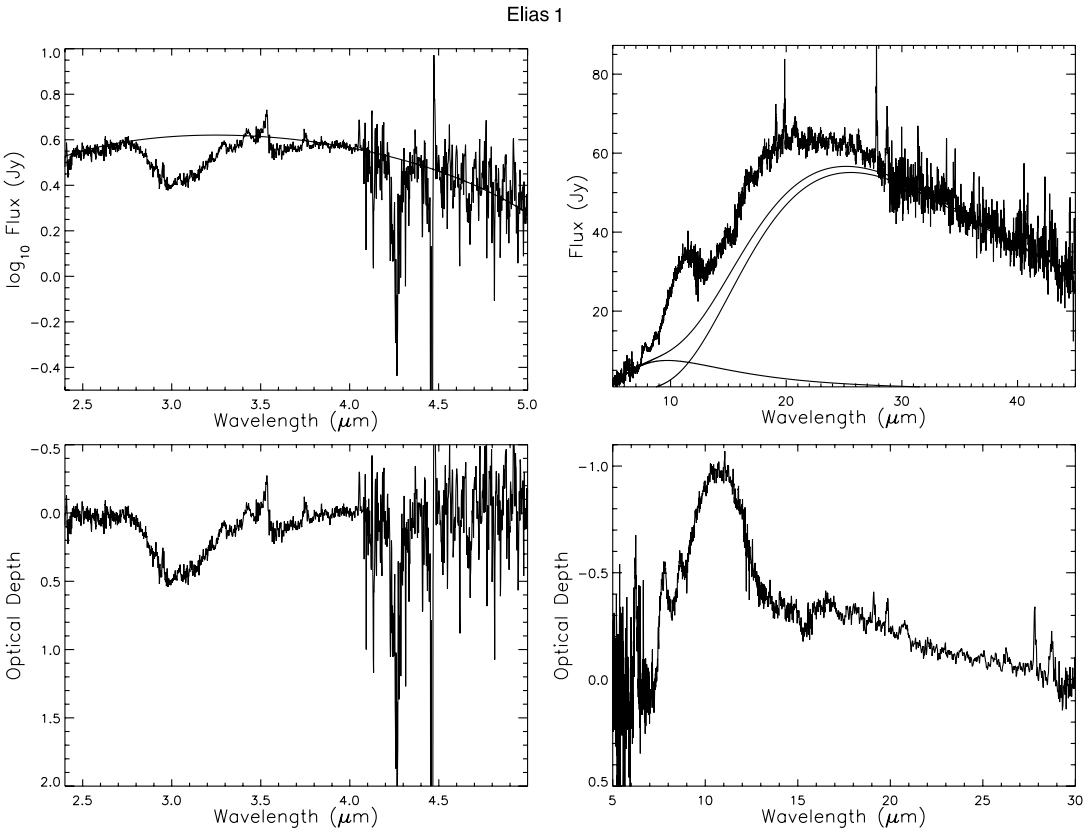

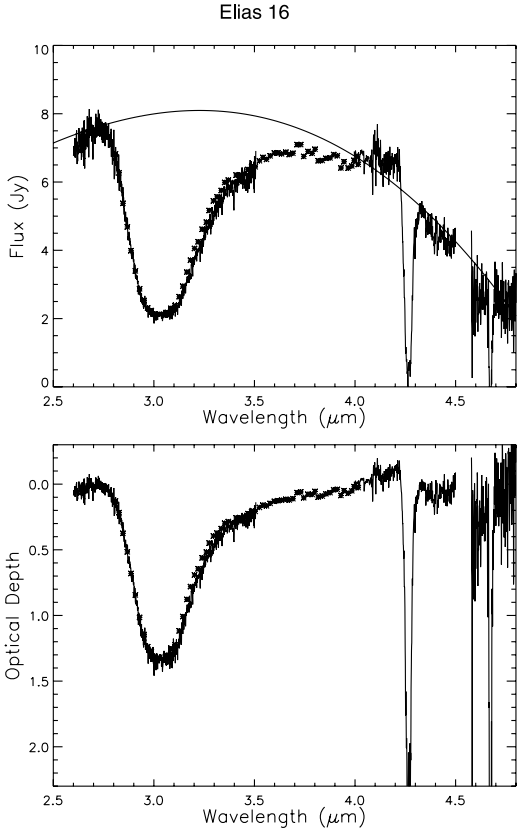

FIG. 1.—*Continued*

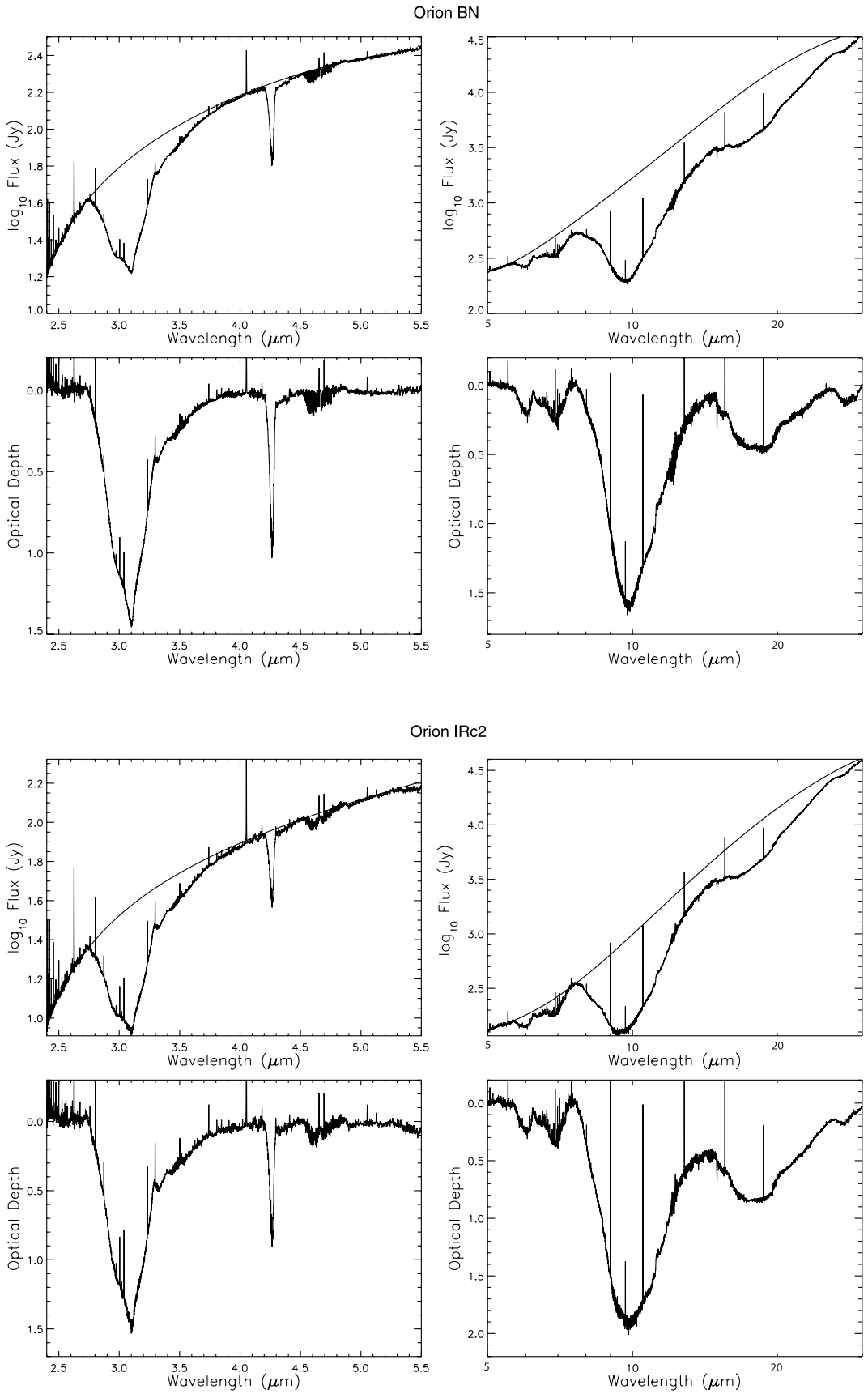

FIG. 1.—*Continued*

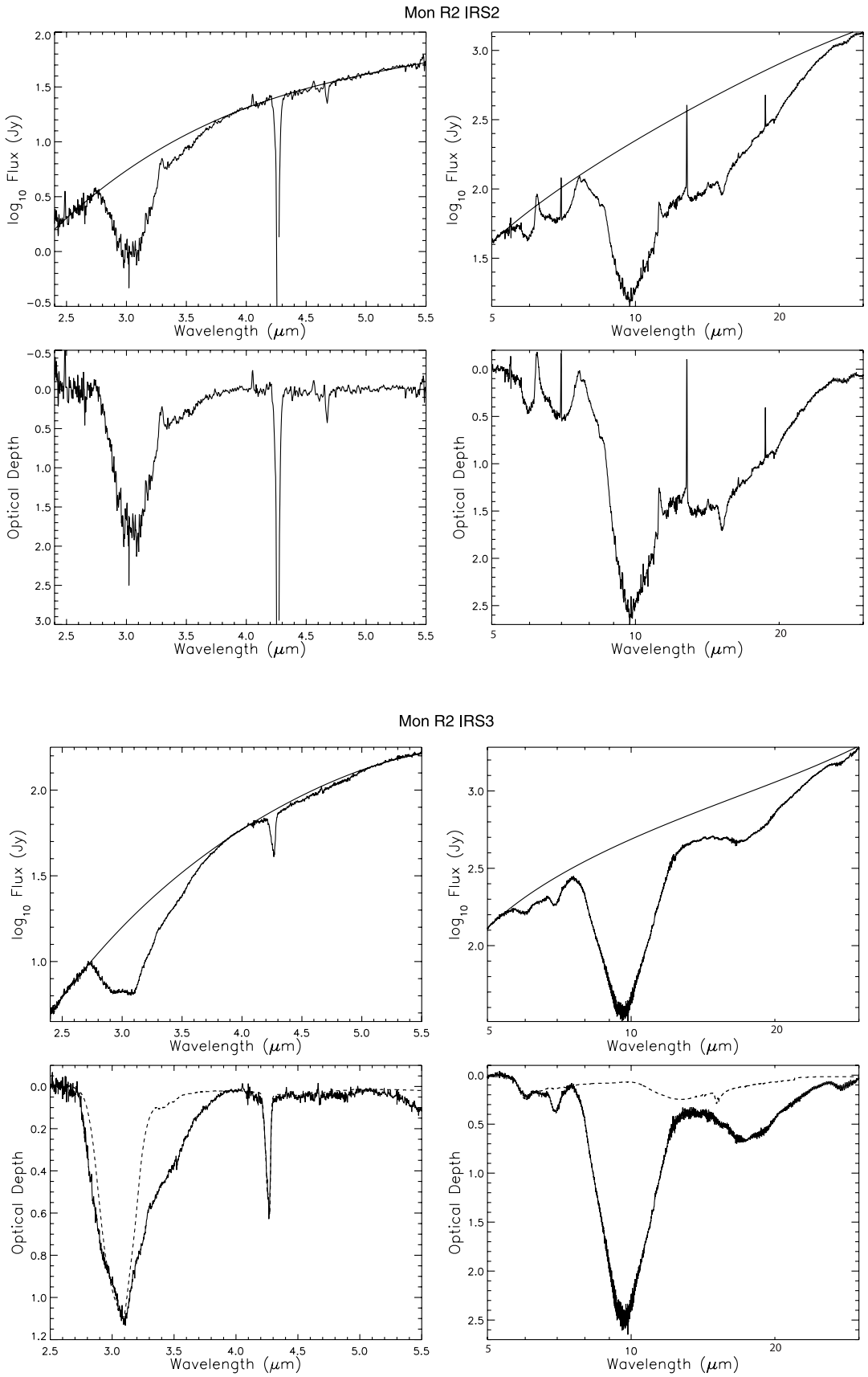

FIG. 1.—*Continued*

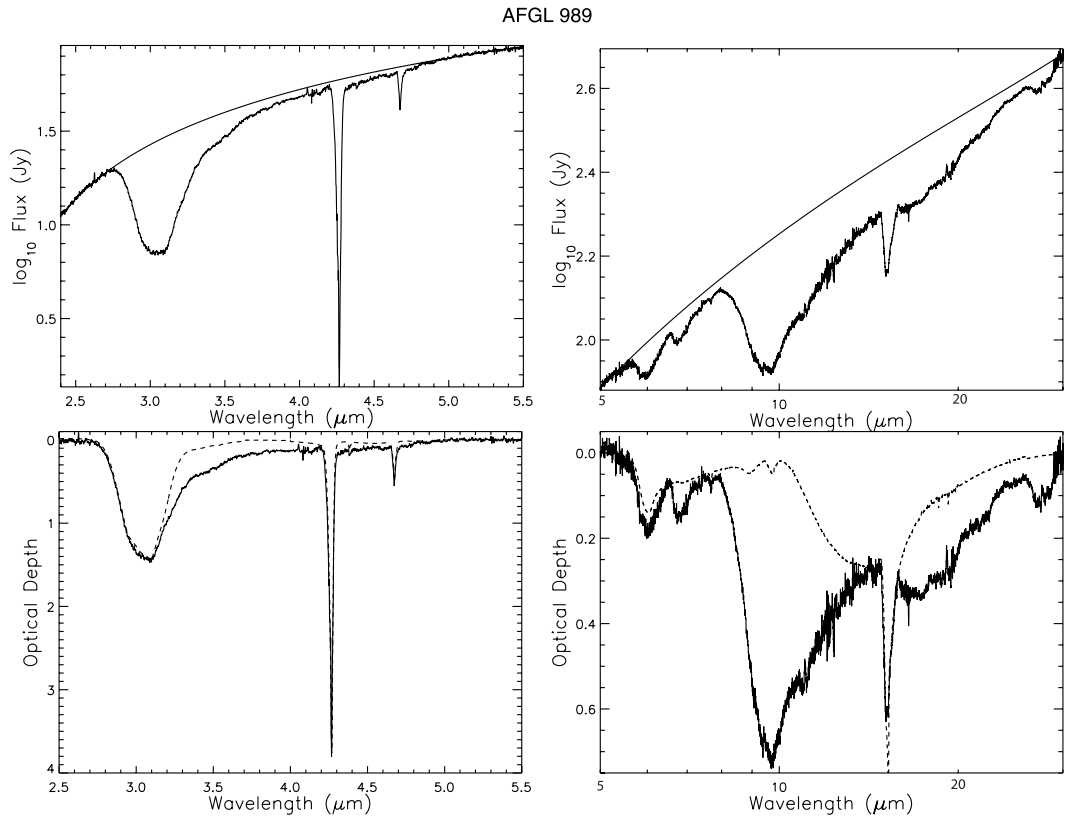

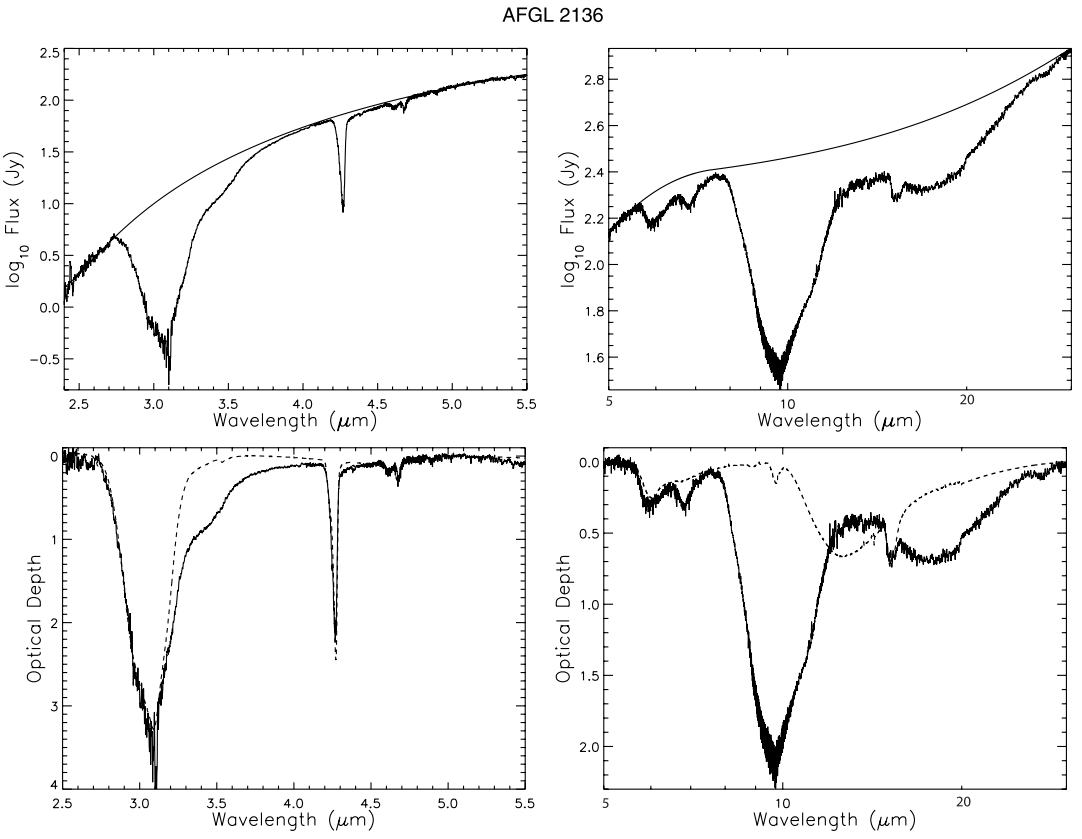

FIG. 1.—*Continued*

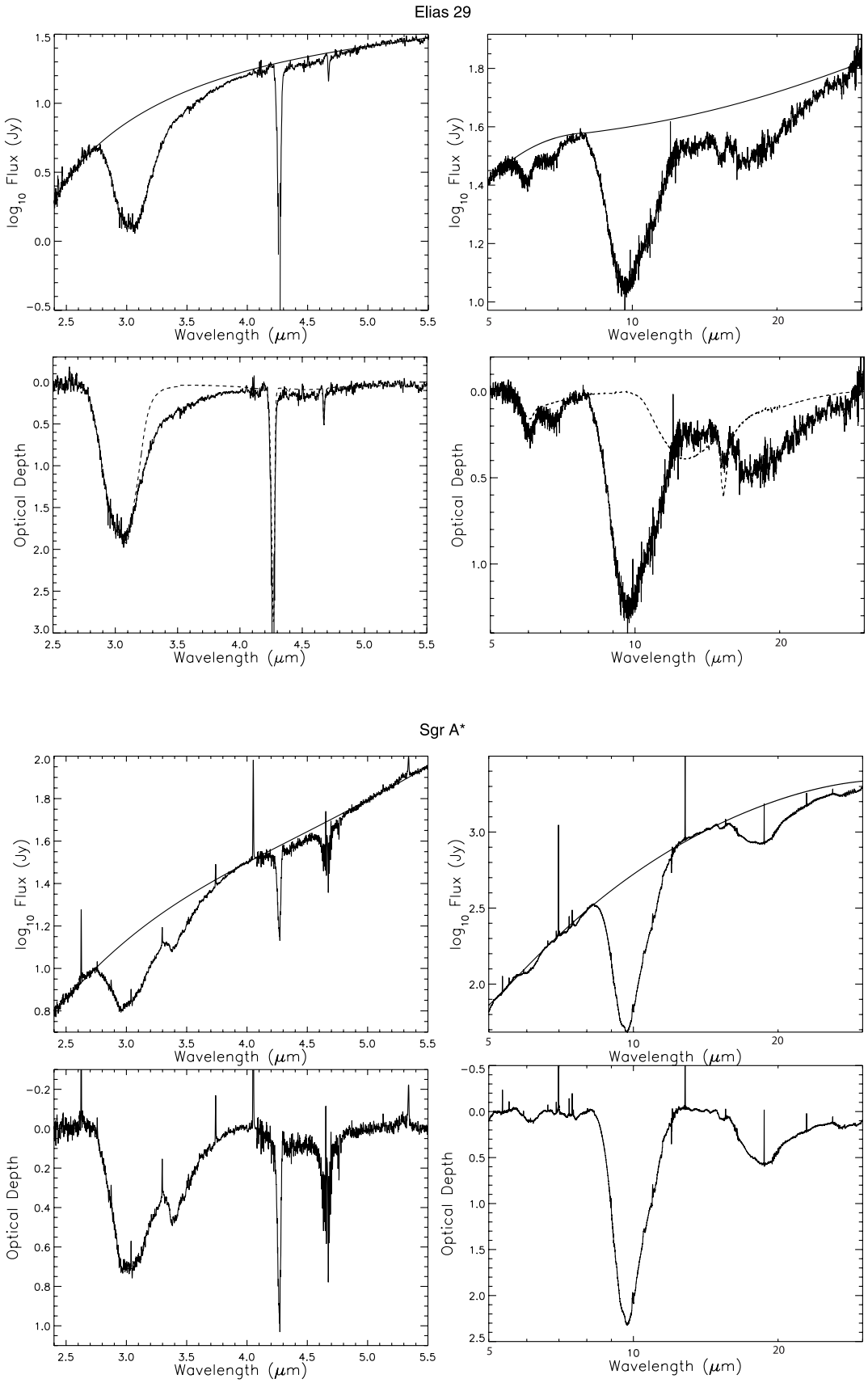

FIG. 1.—*Continued*

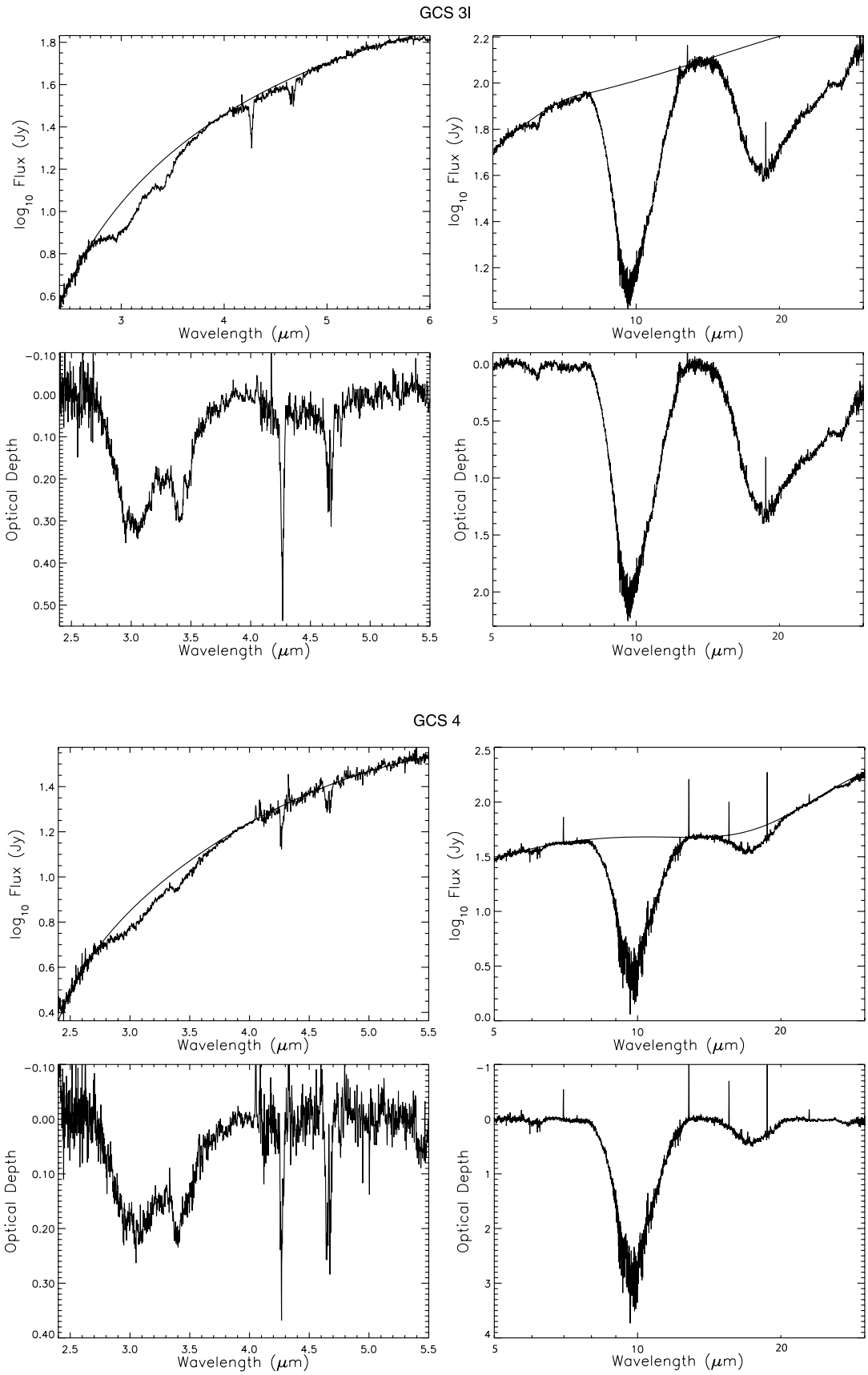

FIG. 1.—*Continued*

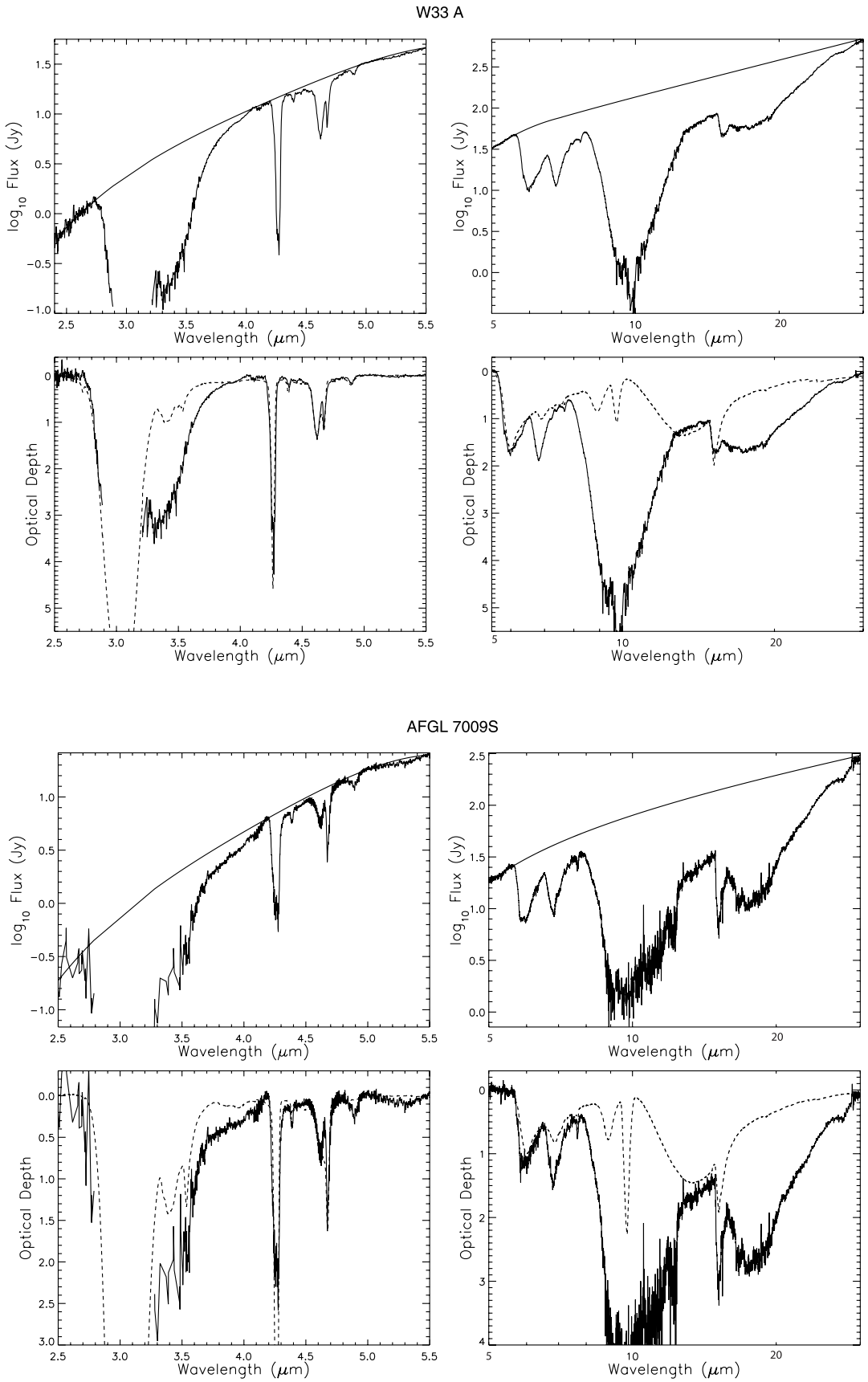

FIG. 1.—*Continued*

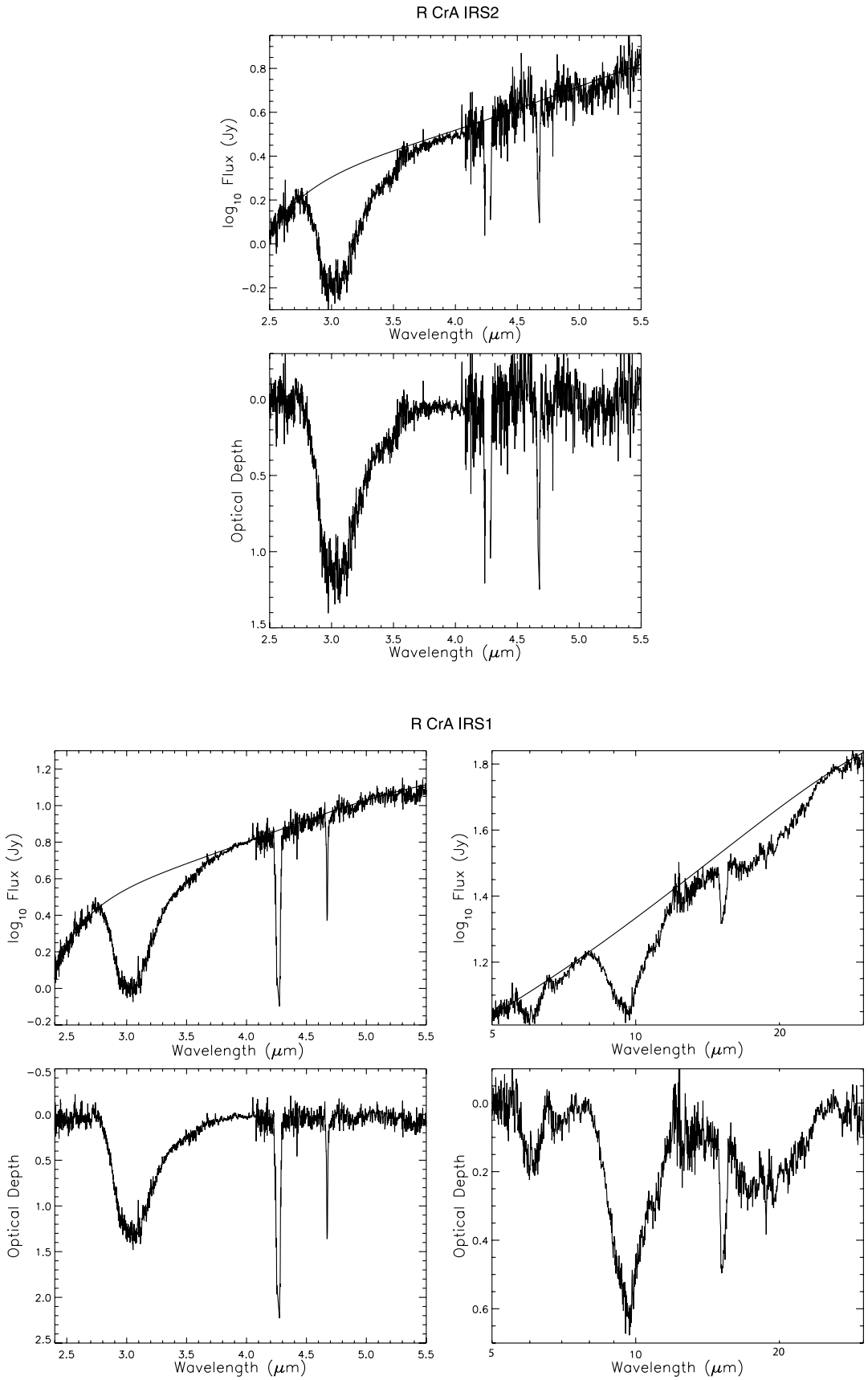

FIG. 1.—*Continued*

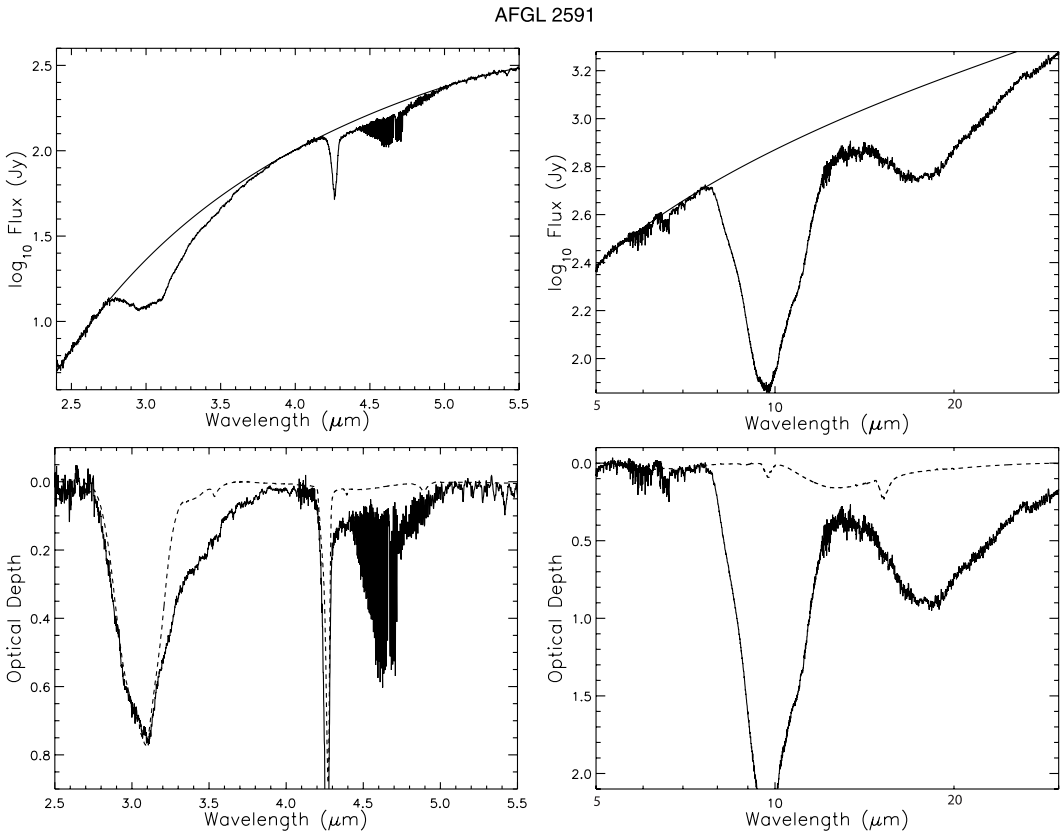

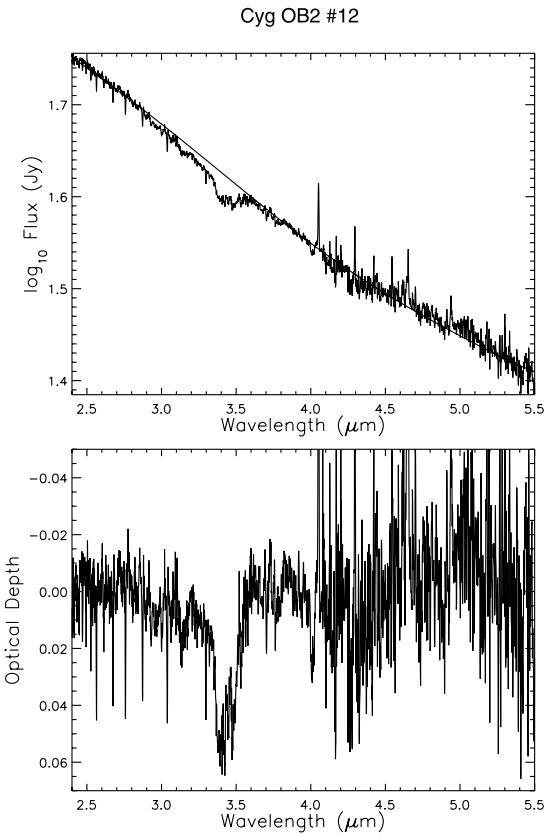

FIG. 1.—*Continued*

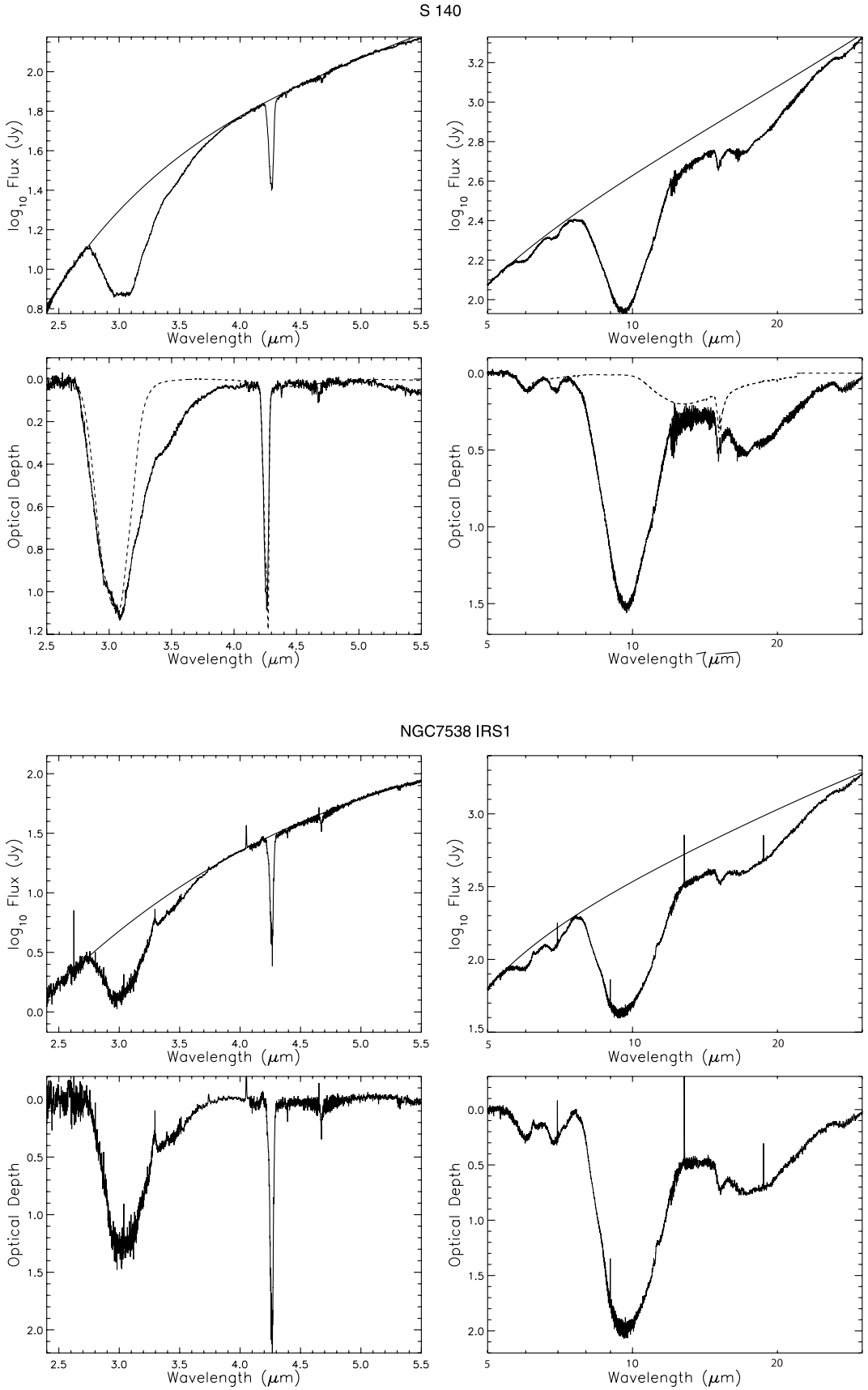

FIG. 1.—*Continued*

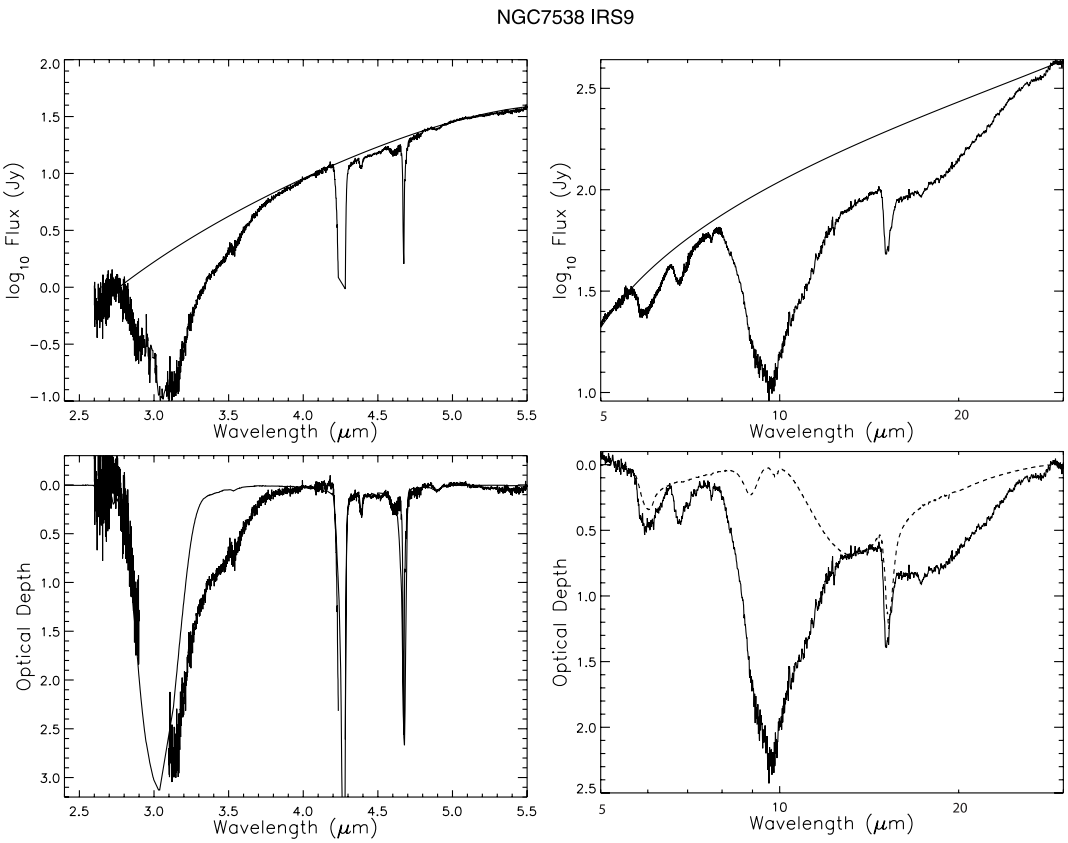

FIG. 1.—*Continued*

complex located in the Perseus arm, 2.3 kpc away (Georgelin & Georgelin 1976). Ongoing star formation is indicated by intense OH and H_2O maser emission and outflows. Tieftrunk et al. (1997) estimated that if each hypercompact continuum source is being ionized by a single stellar object, then they are of ZAMS spectral type B1–B3. The infrared spectrum exhibits emission features due to Ne III, S III, and Si II, as well as the 3.3 μm PAH emission. In addition to this, gas phase absorption lines attributed to warm ($T_{ex} \approx 400$–500 K) C_2H_2, HCN, CO, and H_2O are present (Lahuis & van Dishoeck 2000; Boonman et al. 2003). Molecular abundances of gas phase species toward this source are unusually low, except for sulfur-bearing species (Lahuis & van Dishoeck 2000). The *ISO* spectrum shows strong H_2O and CO_2 features, but the CO ice feature is weak. Absorptions associated with CH-bearing molecules are present at 3.46 and 6.8 μm, but other species have only upper limits.

4.2. *AFGL 490*

AFGL 490 is a $\sim$2200 $L_\odot$ YSO (Mozurkewich, Schwartz, & Smith 1986) in an isolated star-forming region about 1 kpc away (Snell et al. 1984), lying behind 17–50 mag of visual extinction (Rieke & Lebofsky 1985). Radio observations show evidence of outflows of stellar wind (Mitchell et al. 1995). The *ISO* spectrum of this source shows a low column density of ice species along this line of sight along with numerous H I emission lines. Most upper limits are not well constrained because of the low ice column density. Both CO and CO_2 are well fit by purely polar mixtures, whereas most high-mass star formation regions have a significant apolar component.

4.3. *Elias 1*

Elias 1 is classified as a Herbig Ae star (Elias 1978) located behind $\sim$10.5 mag of extinction (Teixeira & Emerson 1999) in the Taurus-Auriga complex. The *ISO* spectrum exhibits silicate and PAH emission features in addition to absorption features of H_2O, CO, and CO_2. The silicate emissivity is broader than the Trapezium emissivity traditionally used to represent molecular cloud material and is also different from that found in comets, peaking at a longer wavelength and differing in overall shape. Hanner, Brooke, & Tokunaga (1994) found that the silicate emissivity can be fit by optically thin 1.5 μm grains, indicating grain growth, though they do not rule out the possibility of a different silicate composition to account for the variation. Emission features at 11.06 and 11.22 μm are seen in both *ISO* and ground-based spectra and may be attributable to crystalline silicates and aromatic hydrocarbons, respectively. There is no evidence in the *ISO* spectrum of the 11.6 and 11.76 μm features tentatively identified in ground-based spectra by Hanner et al. (1994).

4.4. *Elias 16*

Elias 16 is a K1 III giant located behind the Taurus Molecular Cloud and about 23.5 mag of visual extinction (Teixeira & Emerson 1999). The ices in the line of sight are believed to be free from the influence of massive star formation and may therefore represent material unmodified by energetic processing. Because of the intrinsic faintness of this source, SWS only obtained useful data in limited spectral regions between 2.5 and 5 μm. Ground-based data, which match well in flux level, have been used to fill in some regions not

TABLE 3

LABORATORY ICE FITS USED TO FIT SPECTRA IN FIG. 1

Source	Water	CO_2	CO	CH_3OH	OCS	NH_3	CH_4
W3 IRS 5	H_2O 10 K	H_2O:CH_3OH:CO_2 1:1:1 136 K	CO:CO_2 100:8 10 K				
		H_2O:CO_2 100:14 10 K					
Mon R2 IRS 3	H_2O 10 K	H_2O:CO_2:CO 100:20:3 20 K					
	H_2O 175 K	H_2O:CO_2 1:100 10 K					
AFGL 989	H_2O 10 K	H_2O:CO_2 100:14 10 K	H_2O:CO:NH_3 100:23:21 10 K	CH_3OH 10 K	H_2O:OCS 2:1 100K	H_2O:NH_3 100:6 12 K	CH_4 10 K
	H_2O 175 K	H_2O:CO:CO_2 1:50:56 45 K	CO:O_2:CO_2 100:11:20 30 K				
AFGL 2136	H_2O 10 K	H_2O:CO:CO_2 100:3:20 20 K	H_2O:CO_2:CO 100:20:3 20 K	CH_3OH 10 K	H_2O:OCS 2:1 100 K		CH_4 10 K
	H_2O 175 K	H_2O:CH_3OH:CO_2 1:1:1 117 K	H_2O:CO:O_2 1:50:50 10 K				
Elias 29	H_2O 10 K	H_2O:CO_2 100:14 30 K	H_2O:CO_2:CO 100:20:3 20 K				
		H_2O:CH_3OH:CO_2 1:1:1 117 K	H_2O:CO:O_2 1:20:60 30 K				
W33 A	H_2O 50 K	H_2O:CO_2 100:14 10 K	Pure CO	H_2O:CH_3OH:CO_2 1.25:1.2:1.0 70 K	H_2O:OCS 2:1 100 K	H_2O:NH_3 100:9 50 K	H_2O:CH_4 20:1 10 K
		H_2O:CH_3OH:CO_2 1:1:1 112 K	H_2O:CH_3OH +irr 2:1 10 K				
AFGL 7009S	H_2O 50 K	H_2O:CO_2 100:14 10 K	H_2O:CO_2:CO 100:20:3 20 K	CH_3OH 10 K	H_2O:OCS 2:1 100 K	H_2O:NH_3 100:9 50 K	CH_4 10 K
		H_2O:CH_3OH:CO_2 1:1:1 112 K	H_2O:CO:O_2 1:20:60 30 K				
AFGL 2591	H_2O 10 K	H_2O:CO_2 100:14 10 K		CH_3OH 10 K			
	H_2O 175 K	H_2O:CH_3OH:CO_2 1:1:1 117 K					
S140	H_2O 10 K	H_2O:CO_2 100:14 10 K					
	H_2O 175 K	H_2O:CH_3OH:CO_2 1:1:1 136 K					
NGC 7538 IRS 9	H_2O 10 K	H_2O:CO:CO_2 100:3:20 20 K	CO:H_2O 10:1 10 K	H_2O:CH_3OH:CO_2 1.25:1.2:1 10 K	H_2O:OCS 2:1 10 K	H_2O:NH_3 100:9 10 K	
		H_2O:CH_3OH:CO_2 1:1:1 119 K	H_2O:CO 4:1 100 K				

TABLE 4
W3 IRS 5 Spectral Features

λ (μm)	FWHM (cm^{-1})	τ	Species	N (10^{17} cm^{-2})	$N/N(H_2O)$ *100	Reference
3.0	335	2.78(0.19)	H_2O	51(3.5)	100	1
3.29	37		PAH			2
3.461	95	0.133(0.019)	HAC	...	...	3
3.54	30	<0.04	CH_3OH	<1.7	<3.3	2
3.95	115.3	<0.012	CH_3OH	<2.8	<5.6	2
4.27	20	>3	CO_2	7.1(1.8)	13.9(3.5)	4
4.38	8.9	0.073(0.012)	$^{13}CO_2$	0.063(0.013)	0.12(0.025)	5
4.5[a]	700	[0.069]	H_2O	[51]	[100]	2
4.62[b]	28	<0.02	XCN	<0.12	<0.23	2
4.67[b]	6.0	0.24(0.02)	CO	1.6(0.29)	3.1(0.57)	2
		0.07	(Polar)	0.70	1.4	2
		0.17	(Nonpolar)	0.99	1.9	2
4.91	20	<0.04	OCS	<0.05	<0.1	2
5.83	21	<0.05	H_2CO	<0.59	<1.2	2
5.85	65	<0.05	HCOOH	<0.62	<1.2	2
6.02	157	0.26(0.02)	H_2O	51(4)	100(8)	6
6.0		<0.03	Organic residue			2
6.2		<0.02	PAH?	...	...	6
6.85	99	0.22(0.02)	Organics/NH_4^+	...	...	6
7.243	16.8	$\sim$0.028	SO_2 gas	0.5(0.08)	...	7
7.414	17.8	<0.054	SO_2 gas	...	...	7
7.676	10	<0.046	CH_4	<0.67	<1.3	2
9.0	68	<0.055	NH_3	<2.9	<5.7	1
9.7	218	$\sim$5.8	Silicate	...	...	2
9.75	30	<0.36	CH_3OH	<6.4	<12.5	2
13.3[a]	240	[1.30]	H_2O	[51]	[100]	2
15.2	24.6	0.37(0.01)	CO_2	7.1(1.8)	13.9(3.5)	4
			(Polar)	6.2	12.2	4
			(Nonpolar)	0.9	1.8	4
18	201	1.29	Silicate	...	...	2

Notes.—The up and down scans in the aot1 spectrum do not match between 6.5 and 8 μm. The down scan matches the aot6 spectrum, so we used that instead. There are emission lines at 15.55 μm (Ne III $^3P_1$—$^3P_2$), 18.71 μm (S III $^3P_2$—$^3P_1$), 33.48 μm (S III $^3P_1$—$^3P_0$), and 34.81 μm (Si II $^2P_{3/2}$—$^2P_{1/2}$).

[a] Calculated from 3 μm feature.

[b] Gas phase CO.

References.—(1) Gibb et al. 2001; (2) this work; (3) Brooke et al. 1996; (4) Gerakines et al. 1999; (5) Boogert et al. 2000; (6) Gibb & Whittet 2002; (7) Keane et al. 2001c.

covered by SWS. The spectrum shows deep absorption attributed to H_2O, CO_2, and CO (Whittet et al. 1998) as well as a weak feature at 3.47 μm attributed to hydrocarbons (Chiar et al. 1996). Stellar photospheric absorption lines of CO and OH are also present. There are low upper limits of CH_3OH (2.9%), XCN (1.5%), and OCS (0.27%) relative to H_2O. This supports the theory that CH_3OH and XCN are formed by thermal or UV processing in the protostellar environments where they are found to be more abundant.

4.5. *Orion BN*

BN is a luminous infrared source ($\sim$2500 $L_\odot$) in the Orion Molecular Cloud complex suffering from $\sim$17 mag of visual extinction (Gezari, Backman, & Werner 1998). It is located about 450 pc away and is probably illuminated by a B3–B4 star (Gezari et al. 1998), though there are many other sources present in the $14'' \times 20''$ *ISO* SWS beam, including Orion IRc2, which is $\sim 8''$ away. Its infrared spectrum is rich in both ice absorption and emission features caused by PAHs, H_2 and H I, and atomic fine structure lines from the foreground photodissociation region (PDR) and H II region (van Dishoeck et al. 1998). The 3.1 μm water-ice feature exhibits narrow spectral structure, indicative of warm temperatures and annealing.

4.6. *Orion Irc2*

Orion Irc2 is another luminous ($\sim$1000 $L_\odot$) object located in the OMC complex behind about 60 mag of visual extinction (Gezari et al. 1998). There are at least four sources within the SWS beam (van Dishoeck et al. 1998). This region is one of the best studied massive star formation regions to date. The environment is complex with powerful, disrupting outflows and intense UV radiation that gives rise to atomic fine structure lines. PAH emission features are present at 3.3, 6.2, 8.6, and 11.3 μm and may originate on the front side of the photon-dominated region (Tielens et al. 1993). In addition to these are ice absorption features due to H_2O, CO_2, and other minor constituents and gas phase absorption features due to CO, C_2H_2, HCN, and CO_2. There are also over a dozen rotational lines of H_2O in absorption in the 25–45 μm region and OH lines at 28.94 and 34.6 μm, which probably originate in the shocked plateau (van Dishoeck et al. 1998).

4.7. *Mon R2 IRS 2*

Mon R2 is a massive star formation region located 950 pc from the Sun. Most of the infrared cluster, including IRS 2, appears to be on the far side of the molecular cloud (Choi et al. 2000). IRS 2 is located within a hole in the molecular

TABLE 5
AFGL 490 Spectral Features

λ (μm)	FWHM (cm^{-1})	τ	Species	N (10^{17} cm^{-2})	$N/N(H_2O)$ *100	Reference
3.0.....	432	0.32(0.01)	H_2O	6.2(0.3)	100	1
3.46.....	121	0.03	HAC	...	...	2
3.54.....	30	<0.015	CH_3OH	<1.25	<20	2
3.95.....	115	<0.004	CH_3OH	<1.26	<20	2
4.27.....	21.3	0.46(0.05)	CO_2	1.7(0.3)	27(5)	3
4.38.....	12.9	<0.056	$^{13}CO_2$	<0.099	<1.6	2
4.5[a]	700	[0.009]	H_2O	[6.2]	[100]	2
4.62[b]	29	<0.025	XCN	<0.077	<1.2	2
4.67.....	4.15	0.34(0.03)	CO	1.56(0.13)	25.1(2.4)	2
		<0.02	(Polar)	<0.25	<4	2
		0.33	(Nonpolar)	1.53	24.6	2
4.91.....	20	<0.02	OCS	<0.026	<0.42	4
6.02[a]	185	[0.034]	H_2O	[6.2]	[100]	
6.0.....		0.04(0.02)	Organic residue	...	...	2
6.85.....	88	0.05(0.02)	Organics/NH_4^+	...	...	2
7.25.....	16.8	<0.018	HCOOH	<1.2	<19	2
7.414.....	17.8	<0.018	$HCOO^-$	<0.20	<3.2	2
	10.6	<0.018	CH_3HCO	<1.3	<21	2
7.676.....	7.70	<0.013	CH_4	<0.15	<2.4	2
8.90.....	34	[~0.003]	CH_3OH	[~0.69]	[11]	2
9.0.....	68	<0.02	NH_3	<1.0	<16	1
9.7.....	211	0.64(0.02)	Silicate	...	...	2
9.75.....	30	0.039(0.014)	CH_3OH	0.69(0.25)	11(4)	2
13.3[a]	240	[0.082]	H_2O	[6.2]	[100]	2
15.2.....	22.2	0.08(0.02)	CO_2	1.7(0.3)	27(5)	3
			(Polar)	1.7	27	3
			(Nonpolar)	<0.1	<1.6	3
18.....	122	0.16(0.01)	Silicate	...	...	2

Note.—There are emission lines at 2.626 μm (Brβ), 4.052 μm (Brα), 2.675 μm (Pfθ), 2.7572 μm (Pfη) 2.8719 μm (Pfζ), 3.037 μm (Pfϵ), and 3.296 μm (Pfδ).

[a] Calculated from 3 μm feature.

[b] Gas phase CO.

References.—(1) Gibb et al. 2001; (2) this work; (3) Gerakines et al. 1999; (4) Palumbo et al. 1997.

emission and coincident with an H II region (IRS 1), greatest molecular densities occurring just beyond the boundaries of the H II region. The infrared spectrum shows strong PAH emission features along with atomic fine structure emission. H_2O and CO_2 are the principle ice components, though XCN, CH_3OH, and CO are also present.

4.8. *Mon R2 IRS 3*

Mon R2 IRS 3, one of the brightest thermal infrared sources in the galaxy, is another massive star-forming region in the Mon R2 core. It is associated with the brightest and most highly variable OH 4765 MHz maser in the sky as well as the strongest H_2O and CH_3OH masers in the Mon R2 region (Smits, Cohen, & Hutawaradorn 1998). There is evidence of a molecular outflow associated with the maser and circumstellar disk (Koresko et al. 1993). IRS 3 is the most active center of star formation in Mon R2 and unlike the other sources in the infrared cluster, IRS 3 appears to be on the nearside of a dense clump of molecular material (Choi et al. 2000). The peak of its 3 μm H_2O feature is narrow and shifted, indicating that most of the ice along the line of sight is warm (~80 K) and has undergone annealing. This spectrum is unusual in that it has very deep excess absorption on both short- and long-wavelength wings of the water feature (Smith, Sellgren, & Tokunaga 1989) with a profile that is not matched by any other known sources. This excess has yet to be explained but may be caused by a combination scattering and absorption by CH-bearing molecules. Most of the CO in this source has been evaporated, which is not surprising given the high water temperatures. Keane et al. (2001b) reported gas phase SO_2 in absorption toward this and other YSOs.

4.9. *AFGL 989*

AFGL 989 is an intermediate-mass YSO surrounded by embedded low-mass stars (Schreyer et al. 1997) located in the NGC 2264 molecular cloud complex near the apex of the Cone Nebula at a distance of 800 pc (Wynn-Williams 1982). It is also known as NGC 2264 IRS 1 and Allen's source. The luminosity (Henning, Pfau, & Altenhoff 1990, 3.3×10^3 $L_\odot$) is consistent with a 9.5 $M_\odot$ B2 zero-age main-sequence star (Allen 1972) with 20–30 mag of visual extinction (Thompson et al. 1998). This source has an unusually high abundance of CO_2, ~34%, (Nummelin et al. 2001) about twice the average found by Gerakines et al. (1999) in a variety of sources from high-mass YSOs to background field stars.

4.10. *AFGL 2136*

AFGL 2136 is a luminous, 7×10^4 $L_\odot$ source at a distance of about 2 kpc. This source is associated with a bipolar reflection nebula that suggests the presence of a circumstellar disk as well as intense H_2O maser emission (Minchin et al. 1991). Low abundances of apolar ice species (Sandford et al.

TABLE 6
Elias 1 Spectral Features

λ (μm)	FWHM (cm^{-1})	τ	Species	N (10^{17} cm^{-2})	$N/N(H_2O)$ *100	Reference
3.0	358	0.51(0.04)	H_2O	9.2(1.4)	100	1, 2
3.29	44.6	...	PAH emission	...	...	1
3.42	34	−0.24(0.02)	HAC	...	...	3
3.54	24	−0.40(0.02)	?	...	...	3
4.27	12.5	1.5(0.5)	CO_2	4.8(1.6)	52(19)	1
4.38	10	<0.15	$^{13}CO_2$	<0.20	<2.2	1
4.5[a]	700	[0.013]	H_2O	[9.5]	[100]	1
4.62	28	<0.16	XCN	<0.95	<10	1
4.674	9.48	0.14	CO	0.8(0.2)	8.7(2.4)	4
		0.04(0.03)	(Polar)	0.3(0.2)	3.3(2.4)	4
		0.10(0.03)	(Apolar)	0.5(0.2)	5.4(2.4)	4
4.91	20	<0.13	OCS	<0.16	<1.7	1
6.02[b]	185	...	H_2O	...	...	
6.23	65	...	PAH emission	...	...	3
6.85[b]	88	...	Organics	...	...	
7.74	79	...	PAH emission	...	...	1
8.61	35.7	...	PAH emission	...	...	1
9.7	324	−1.0(0.05)	Silicate	...	...	1
11.3		...	PAH emission	...	...	3
13.3[a]	240	[0.086]	H_2O	[9.5]	[100]	1
15.2	22	0.14(0.02)	CO_2	3.0(0.9)	33(11)	1

Note.—There is an emission line at 4.05 μm (Brα).
[a] Calculated from 3 μm feature.
[b] Poor S/N, PAH emission.
References.—(1) This work; (2) Whittet et al. 1983; (3) Hanner et al. 1994; (4) Chiar et al. 1995.

1988; Schutte et al. 1996) and modeling of submillimeter flux densities (van der Tak et al. 1999) indicate that dust and gas temperatures of ≈30 K dominate along most of the line of sight. This is consistent with the shape of the 3 μm water profile as well as the 9.75 μm CH_3OH feature, which is best fitted by a pure 50 K methanol laboratory spectrum. Mitchell et al. (1990) find that while most of the CO gas is hot (∼580 K), there is also a substantial cold (∼17 K) component. Likewise, Boonman et al. (2003) and Lahuis & van Dishoeck (2000) find substantial column densities of hot (500–800 K) H_2O, C_2H_2, and HCN gas with only a small cold gas component.

4.11. *Elias 29*

Elias 29 is a low-mass (36 $L_\odot$) class I protostar located behind ∼47.8 mag of visual extinction (Teixeira & Emerson 1999) in the ρ Oph molecular cloud at a distance of ∼160 pc. This source is ideal for studying processes in low-mass star formation regions as it is one of the most luminous protostars in the ρ Oph cloud (Chen et al. 1995). The full 2.3–190 μm

TABLE 7
Elias 16 Spectral Features

λ (μm)	FWHM (cm^{-1})	τ	Species	N (10^{17} cm^{-2})	$N/N(H_2O)$ *100	Reference
2.96			NH_3		<10	1
3.0	335	1.36(0.03)	H_2O	25(0.6)	100	1,2
3.25		<0.029	C-H stretch	...	...	3
3.47	60	0.032(0.002)	HAC	...	...	2
3.54	30	<0.02	CH_3OH	<0.72	<2.9	2
4.27	19.6	1.8(+0.5, −0.2)	CO_2	4.6(+1.3, −0.6)	24.2(6.8, −3.2)	4
			(Polar)	4.6	24.2	4
			(Apolar)	<0.2	<0.8	4
4.38	8.5	0.060(0.017)	$^{13}CO_2$	0.047(0.015)	0.19(0.08)	5
4.5[a]	700	[0.036]	H_2O	[25]	[100]	1
4.62	28	<0.05	XCN	<0.28	<1.5	6
4.67	4.75	1.31(0.03)	CO	6.5(0.3)	25	7
		0.11(0.03)	(Polar)	0.8(0.2)		
		1.22(0.03)	(Apolar)	5.6(0.1)		
4.91	20	<0.04	OCS	<0.052	<0.27	8

[a] Calculated from 3 μm feature.
References.—(1) Gibb et al. 2001; (2) Chiar et al. 1996; (3) Sellgren et al. 1994; (4) Gerakines et al. 1999; (5) Boogert et al. 2000; (6) Whittet et al. 2001; (7) Chiar et al. 1995; (8) Palumbo et al. 1997.

TABLE 8
ORION BN SPECTRAL FEATURES

λ (μm)	FWHM (cm^{-1})	τ	Species	N (10^{17} cm^{-2})	$N/N(H_2O)$ *100	Reference
3.0	353	1.44(0.04)	H_2O	25(0.7)	100	1
3.3	...	...	PAH emission	...	...	
3.459	78	0.034	HAC	...	...	2
3.53	29	<0.02	CH_3OH	<0.9	<4	3
3.95	115.3	<0.03	CH_3OH	<6.8	<27	3
4.27	21.6	0.96(0.04)	CO_2	2.9(0.1)	11.6(0.5)	3
			(Polar)	0.97	3.9	3
			(Nonpolar)	1.93	7.7	3
4.38	9.5	<0.021	$^{13}CO_2$	<0.037	<0.15	3
4.5[a]	700	[0.034]	H_2O	[25]	[100]	
4.62[b]	28	<0.04	XCN	<0.24	<0.95	3
4.67[b]	...	...	CO	...	...	
4.91	19.6	<0.016	OCS	<0.02	<0.08	3
6.02[a]	172	[0.073]	H_2O	[25]	[100]	
6.0		0.17(0.01)	Organic residue	...	...	3
6.2	60	...	PAH emission	...	...	
6.85	79	0.28(0.02)	Organics/NH_4^+	...	...	3
7.243	16.9	0.04(0.01)	HCOOH	2.4(0.6)	9.4(2.4)	3
			$HCOO^-$	0.77(0.2)	3.1(0.8)	3
7.414	17.8	<0.052	$HCOO^-$	<0.58	<2.3	3
	10.6		CH_3HCO	<3.9	<16	3
7.676	10.4	<0.028	CH_4	<0.42	<1.7	3
9.0	68	<0.05	NH_3	<2.5	<10	1
9.7	304	1.59(0.02)	Silicate	...	...	3
13.3[a]	240	[0.22]	H_2O	[25]	[100]	
13.7			C_2H_2 gas	...	...	
14			HCN gas			
15.24[c]	27.4	0.07(0.02)	CO_2	1.9(0.5)	7.6(2.2)	3
18	160	0.45(0.02)	Silicate	...	...	3

NOTE.—There are emission features at 2.4065 μm (H_2? 1–0), 2.4137 μm, 2.4238 μm (H_2 1–0 $Q(3)$), 2.4377 μm, 2.4548 μm, 2.4758 μm, 2.5004 μm, 2.625 μm (Brβ), 2.676 μm, 2.803 μm, 2.873 μm (Pfζ), 2.974 μm, 3.004 μm, 3.038 μm (Pfϵ), 3.235 μm (H_2 1–0 $O(5)$), 3.296 μm (Pfδ), 3.501 μm, 3.739 μm (Pfγ), 3.808 μm, 3.847 μm, 3.908 μm, 4.051 μm (Brα), 4.652 μm (Pfβ), 4.695 μm, 5.052 μm, 5.512 μm (H_2 $S(7)$), 6.488, 6.523, 6.573, 6.594, 6.636 μm (Ni II $^2D_{3/2}$–$^2D_{5/2}$?), 6.676, 6.709, 6.724, 6.794, 6.829, 6.865, 6.911, 6.985 μm (Ar II $^2P_{1/2}$–$^2P_{3/2}$), 7.05, 7.348 μm (SO_2), 7.461 (H I 6–5), 7.66 μm (CH_4), 8.991 μm (Ar III $^3P_1$–$^3P_2$), 9.665 (H_2?), 10.510 μm (S IV $^2P_{3/2}$–$^2P_{1/2}$), 12.814 μm (Ne II $^2P_{1/2}$–$^2P_{3/2}$), 15.555 μm (Ne III $^3P_1$–$^3P_2$), 18.713 μm (S III $^3P_2$–$^3P_1$), 25.249 μm (SI $^3P_1$–$^3P_2$), 33.48 μm (S III $^3P_1$–$^3P_0$), and 34.819 μm (Si II $^2P_{3/2}$–$^2P_{1/2}$).

[a] Calculated from 3 μm feature.

[b] Gas phase CO.

[c] Affected by fringing.

REFERENCES.—(1) Gibb et al. 2001; (2) Brooke et al. 1996; (3) this work.

spectrum was studied in detail by Boogert et al. (2000). This source has a somewhat unusual spectral energy distribution that is very flat up to $\sim$100 μm. While hot ($\sim$500 K) H_2O and CO gas have been observed, the ices do not show signs of thermal processing. There is also evidence of PAH material with absorptions at 3.25, 3.49, and possibly 6.2 μm.

4.12. *Sgr A**

Sgr A* is a Galactic center (GC) source suffering $\sim$30 mag of visual extinction (Lutz et al. 1996), which arises from both diffuse and dense regions of the ISM (Chiar et al. 2002). The $14'' \times 20''$ SWS beam included H II regions, M giants, and supergiants. The infrared spectrum has a strong absorption feature at 2.96 μm, suggestive of the N-H stretch feature in NH_3, but whose true nature is unknown (Chiar et al. 2000; Gibb et al. 2001). Other features include prominent H_2O, CO_2, and CH_4-ice absorption, and HAC absorption features at 3.4, 6.2, 6.8, and 7.25 μm (Chiar et al. 2000). Moneti, Cernicharo, & Pardo (2001) find that most of the water along the line of sight is in the solid phase, originating in dense molecular clouds, and that most of the H_2O that is in the gas phase is cold, consistent with the conclusion of Gerakines et al. (1999) that most of the CO_2 along the line of sight is colder than 50 K.

4.13. *GCS 3I and GCS 4*

GCS 3I and GCS 4 are in a region located approximately 40 pc from the Galactic center near the GC Radio Arc. These sources are believed to lie behind $\sim$29 mag of visual extinction and are in a region known as the Infrared Quintuplet, containing several bright and many faint IR sources whose nature is still unknown (Chiar et al. 2000). Both spectra exhibit atomic fine structure lines. As with Sgr A*, these lines of sight intercept both dense clouds and diffuse-ISM dust. Ices in the dense-cloud component are represented by features of H_2O, CO_2, and CO, whilst hydrocarbon features at 3.28, 3.4, 6.2 and 6.8 μm arise in either diffuse-ISM or circumstellar material. The GC sources also show excess absorption near 2.95 μm that might be indicative of NH_3 along the line of sight (Chiar et al. 2000).

4.14. *W33 A*

W33 A is a massive, luminous (1.1×10^5 $L_\odot$) YSO located $\sim$4 kpc from the Sun in the W33 H II molecular cloud

TABLE 9
ORION IRc2 SPECTRAL FEATURES

λ (μm)	FWHM (cm^{-1})	τ	Species	N (10^{17} cm^{-2})	$N/N(H_2O)$ *100	Reference
3.0	335	1.48(0.02)	H_2O	24.5(0.3)	100	1
3.3	...	...	PAH emission	...	...	
3.53[a]	29	0.06(0.02)	CH_3OH	2.5(0.8)	10(3)	1
4.27[a]	19.6	0.9(0.1)	CO_2	2.6(0.3)	10.6(1.2)	1
			(Polar)	0.7	2.9	1
			(Nonpolar)	1.9	7.8	1
4.38	9.5	0.06(0.01)	$^{13}CO_2$	0.078(0.013)	0.32(0.05)	1
4.5[b]	700	[0.03]	H_2O	[24.5]	[100]	
4.62	28	$\sim$0.08	XCN	0.48	2.0	1
4.67[c]	7.64	...	CO	...	...	
4.91	23	<0.03	OCS	<0.04	<0.2	1
6.02[b]	172	[0.07]	H_2O	[24.5]	[100]	
6.0		0.17(0.02)	Organic residue	...	...	1
6.2	60	...	PAH emission	...	...	
6.85	79	0.32(0.02)	Organics/NH_4^+	...	...	1
7.676[d]	10.4	...	CH_4	...	...	
9.7	297	1.87(0.05)	Silicate	...	...	1
13.3[b]	240	[0.22]	H_2O	[24.5]	[100]	
15.24[e]	27.4		CO_2			
18	213	0.75(0.02)	Silicate	...	...	1

NOTE.—There are emission features at 2.4065 μm (H_2? 1–0), 2.4137 μm, 2.4238 μm (H_2 1–0 $Q(3)$), 2.4377 μm, 2.4548 μm, 2.4758 μm, 2.5004 μm, 2.625 μm (Brβ), 2.676 μm, 2.803 μm, 2.873 μm (Pfζ), 2.974 μm, 3.004 μm, 3.038 μm (Pfϵ), 3.235 μm (H_2 1–0 $O(5)$), 3.296 μm (Pfδ), 3.501 μm, 3.739 μm (Pfγ), 3.808 μm, 3.847 μm, 3.908 μm, 4.051 μm (Brα), 4.652 μm (Pfβ), 4.695 μm, 5.052 μm, 5.512 μm (H_2 $S(7)$), 6.488, 6.523, 6.573, 6.594, 6.636 μm (Ni II $^2D_{3/2}$—$^2D_{5/2}$?), 6.676, 6.709, 6.724, 6.794, 6.829, 6.865, 6.911, 6.985 μm (Ar II $^2P_{1/2}$—$^2P_{3/2}$), 7.05, 7.348 μm (SO_2), 7.461 (H I 6–5), 7.66 μm (CH_4), 8.991 μm (Ar III $^3P_1$—$^3P_2$), 9.665 (H_2?), 10.510 μm (S IV $^2P_{3/2}$—$^2P_{1/2}$), 12.814 μm (Ne II $^2P_{1/2}$—$^2P_{3/2}$), 15.555 μm (Ne III $^3P_1$—$^3P_2$), 18.713 μm (S III $^3P_2$—$^3P_1$), 25.249 μm (S I $^3P_1$—$^3P_2$), 33.48 μm (S III $^3P_1$—$^3P_0$), and 34.819 μm (Si II $^2P_{3/2}$—$^2P_{1/2}$).

[a] Gase phase lines?
[b] Calculated from 3 μm feature.
[c] Gas phase CO.
[d] Gas phase CH_4 emission.
[e] Gas phase CO_2.

REFERENCES.—(1) This work.

complex and hidden by 50–150 mag of visual extinction (Capps, Gillett, & Knacke 1978; Goss, Matthews, & Winneberg 1978; Mitchell et al. 1990). The infrared spectrum of W33 A is particularly rich, being dominated by deep absorption features attributed to solid H_2O and silicates with detections of sulfur-bearing species (OCS, SO_2), CO, CO_2, $^{13}CO_2$, CH_4, NH_3, and one of the highest abundances of CH_3OH reported to date (Gibb et al. 2000; Dartois et al. 1999). The spectrum also has the deepest 4.62 μm (XCN) and 6.8 μm organic features reported to date as well as a very deep wing longward of the 3.1 μm H_2O feature. Most of the ice along the line of sight is dominated by a cold component, though warmer regions ($\sim$120 K) are also evidenced by a high abundance of CO in the gas phase (Mitchell, Allen, & Maillard 1988; Mitchell et al. 1990), the relative weakness of the pure CO component, and annealing of the 15.2 μm CO_2 feature (Gerakines et al. 1999). Evidence for energetic processing is provided by the presence of abundant CH_3OH and XCN. In addition, W33 A has the deepest excess absorption at 6 μm, which Gibb & Whittet (2002) attribute to an organic refractory component, also formed by energetic processing of icy mantle material. Lahuis & van Dishoeck (2000) report a detection of cold C_2H_2 (10 K) and HCN (80 K) gas.

4.15. *AFGL 7009S*

AFGL 7009S is classified as an ultracompact H II region and is one of the most massive YSOs studied to date, on a par with W33 A. It is a class I YSO, either of late O or early B type. The *ISO* spectrum is similar in many respects to that of W33 A with deep 4.62 and 6.8 μm features. It is also saturated throughout the 3 μm H_2O-ice feature. The H_2O column density was estimated by d'Hendecourt et al. (1996) using both the 6 and 13 μm features. Gibb & Whittet (2002) also report excess absorption at 6 μm attributable to an organic residue, consistent with UV processing of the mantle material.

4.16. *R CrA IRS 2*

The Corona Australis molecular cloud complex is one of the nearest star-forming regions at a distance of $\sim$130 pc (Marraco & Rydgren 1981). Wilking, Taylor, & Storey (1986) identified IRS 2 as one of the protostellar regions based on its spectral energy distribution. It has a bolometric luminosity of $\sim$10 $L_\odot$ and lies behind $\sim$32 mag of extinction. Longward of 5 μm, the SWS spectrum of this source has a high amount of scatter and was not included in the analysis with the exception of an AOT6 observation of the 15.2 μm CO_2 feature.

4.17. *R CrA IRS 1*

R CrA IRS 1, also known as HH100–IR, is an intermediate-mass, pre–main-sequence Herbig Ae star obscured by about 25 mag of visual extinction (Whittet et al. 1996). It is highly variable in the near-infrared and a strong far-infrared source. The profiles of the H_2O and CO ice features are consistent with domination by cold ices, and the lack of a 4.62 μm

TABLE 10
MON R2 IRS 2 SPECTRAL FEATURES

λ (μm)	FWHM (cm^{-1})	τ	Species	N (10^{17} cm^{-2})	$N/N(H_2O)$ *100	Reference
3.0	335	1.77(0.32)	H_2O	35.6(6.4)	100	1
3.3		...	PAH emission	...	...	
3.46	86.1	0.083(0.013)	HAC	...	...	2
3.54	29	0.033(0.010)	CH_3OH	1.3(0.4)	3.7(1.1)	2
4.27	17.7	2.22(0.13)	CO_2	6.02(0.11)	16.9(0.31)	1
4.38	12.9	0.15(0.03)	$^{13}CO_2$	0.26(0.05)	0.73(0.14)	1
4.5[a]	700	[0.048]	H_2O	[35.6]	[100]	1
4.62	23.5	0.05	XCN	0.14	0.39	3, 4
4.67	6.73	0.47(0.02)	CO	2.7(0.2)	7.6(0.6)	5
		0.16(0.02)	(Polar)	1.2(0.2)	3.3(0.6)	5
		0.37(0.02)	(Nonpolar)	1.6(0.1)	4.5(0.3)	5
4.91	23	0.015	OCS	0.013	0.037	6
6.02[a]	150	[0.13]	H_2O	[35.6]	[100]	1
6.0	150	$\sim$0.29	Organic residue	...	...	1
6.2	30	...	PAH emission	...	...	1
6.85	152	0.47(0.04)	Organics/NH_4^+	...	...	1
7.7		...	PAH emission	...	...	
9.7	280	2.54(0.1)	Silicate	...	...	1
11.2	13	...	PAH emission	...	...	1
13.3[a]	240	[0.38]	H_2O	[35.6]	[100]	1
15.2	21.0	0.29(0.02)	CO_2	7.8(0.6)	4.6(1.7)	1
18z		$\sim$1.0	Silicate	...	...	1

NOTE.—There are emission features at 4.051 μm (Brα), 4.652 μm (Pfβ), 6.985 (Ar II $^2P_{1/2}$–$^2P_{3/2}$), 12.814 μm (Ne II $^2P_{1/2}$–$^2P_{3/2}$), 18.713 μm (S III $^3P_2$–$^3P_1$), 33.48 μm (S III $^3P_1$–$^3P_0$), and 34.819 μm (Si II $^2P_{3/2}$–$^2P_{1/2}$).

[a] Calculated based on 3 μm feature.

REFERENCES.—(1) This work; (2) Brooke et al. 1999; (3) Whittet et al. 2001; (4) Demyk et al. 1998; (5) Chiar et al. 1998; (6) Palumbo et al. 1997.

feature is consistent with low levels of energetic processing along most of the line of sight. The 5–30 μm spectral region has been smoothed to a resolving power of 750.

4.18. *AFGL 2591*

AFGL 2591 is a luminous (2×10^4 $L_\odot$), massive (10 $M_\odot$) YSO approximately 1 kpc away behind 70 mag of visual extinction (Carr et al. 1995). This source exhibits the presence of an 11.2 μm polarization feature (Aitken et al. 1988), which may indicate an annealed silicate grain component. This is unusual in dark molecular clouds where the silicate is primarily amorphous in form and requires high temperatures (exceeding 1000 K) to anneal. Mitchell et al. (1990) found that virtually all the CO in this line of sight is in the gas phase with a significant portion at very high temperatures ($\sim$1010 K). Hot H_2O and CO_2 gas absorption lines are also present (Boonman et al. 2003) with temperatures of 450 and 500 K, respectively. In addition to this, Lahuis & van Dishoeck (2000) find very hot (up to $\sim$900 K) C_2H_2 and $\sim$600 K HCN gas phase absorption lines. The 3 μm H_2O-ice feature shows evidence of annealing. However, there is no evidence of an organic refractory mantle component at 6 μm or the 4.62 μm XCN feature thought to indicate processing by UV radiation. Either no such processing has taken place or the processed species have evaporated.

4.19. *Cyg OB2 12*

Cyg OB2 12 is a member of the Cyg OB2 association located $\sim$1.7 kpc away (Torres-Dodgen et al. 1991). This type B5 Ia^+ star, one of the most luminous in the Galaxy, is more reddened than any other member of the association, suffering from 10.2 mag of visual extinction (Humphreys 1978). The obscuring dust appears to be typical of the diffuse ISM (Whittet et al. 1997), and the spectrum of this source is consistent with a stellar photosphere modified by reddening. There are no ices evident in the spectrum, but an absorption feature of silicates at 9.7 μm is present, as well as evidence of hydrocarbons near 3.4 μm. There is no evidence of XCN in this source (Whittet et al. 2001), which indicates that this material is volatile and does not survive diffuse ISM conditions.

4.20. *S140*

S140 is a $\sim$2000 $L_\odot$ H II region located 0.9 kpc away behind $\sim$23 mag of visual extinction (Evans et al. 1989). This region is currently undergoing both high- and low-mass star formation (van der Tak et al. 1999). The infrared spectrum exhibits ice features due to H_2O, CO_2, $^{13}CO_2$, and CH_4. Nearly all the CO is in the gas phase, with both cold (28 K) and warm (390 K) components (Mitchell et al. 1990). Upper limits of a few percent or less were placed on several other species. The shape of the 3.1 μm H_2O peak is indicative of a substantial warm ice component. Only upper limits of gas phase C_2H_2, HCN, CO_2, and H_2O are reported (Lahuis & van Dishoeck 2000; Boonman et al. 2003) with column densities at least an order of magnitude less than those found toward AFGL 2591 and AFGL 2136. The H_2O-ice column densities, on the other hand, are comparable for the three sources (to within about a factor of 3).

4.21. *NGC 7538 IRS 1*

NGC 7538 IRS 1 appears to be the youngest and most luminous (1.3×10^5 $L_\odot$) pre–main-sequence object in the H II regions and molecular clouds that make up the NGC 7538

TABLE 11
Mon R2 IRS 3 Spectral Features

λ (μm)	FWHM (cm^{-1})	τ	Species	N (10^{17} cm^{-2})	$N/N(H_2O)$ *100	Reference
3.0	335	1.12(0.01)	H_2O	19	100	1
3.249	74	0.049(0.007)	PAH, C-H stretch	...	...	2, 3
3.482	76	0.036(0.005)	HAC	...	...	3
3.54	30	<0.022	CH_3OH	<0.92	<4.9	3
4.27	20	0.51(0.03)	CO_2	1.6(0.1)	8.6(0.53)	4
4.38	12.9	<0.018	$^{13}CO_2$	<0.32	<0.17	4
4.5[a]	700	[0.026]	H_2O	[19]	[100]	4
4.62[b]	29	...	XCN	...	...	
4.67[b]	7.64	<0.05	CO	...	...	
4.91	23	<0.01	OCS	<0.013	<0.068	5
5.81	21	<0.04	H_2CO	<1.1	<6	4
5.85	65	<0.04	HCOOH	<0.6	<3	4
6.02	141	0.07(0.02)	H_2O	19(5.4)	100(29)	1
6.0	420	0.15(0.02)	Organic residue	...	...	1
6.85	71	0.32(0.02)	Organics/NH_4^+	...	...	1
7.287	11.45	0.04	SO_2 gas	0.4(0.008)	...	6
7.414	15	0.03	SO_2 gas	0.4(0.008)	...	6
7.676	10.4	<0.016	CH_4	<2.4	<12.8	4
9.0	68	<0.0094	NH_3	<0.49	<2.6	7
9.7	280	2.55(0.09)	Silicate	...	...	4
9.75	30	<0.03	CH_3OH	<0.53	<2.8	4
11.2	22	0.037	PAH, C-H bend	...	...	8
13.3[a]	240	[0.23]	H_2O	[19]	[100]	4
15.2	27.4	0.044(0.003)	CO_2	1.3(0.3)	6.8(1.3)	4
18	217	0.68(0.02)	Silicate	...	...	4

[a] Calculated based on 3 μm feature.
[b] Gas phase CO.
References.—(1) Gibb & Whittet 2002; (2) Brooke et al. 1999; (3) Sellgren et al. 1994; (4) this work; (5) Palumbo et al. 1997; (6) Keane et al. 2001c; (7) Gibb et al. 2001; (8) Bregman et al. 2000.

complex (Strazzulla et al. 1998). It is 2.8 kpc away in the Perseus arm of the galaxy. The SWS spectrum of this source is very rich with PAH, hydrogen, and metal ion emission in addition to absorption features of solid state H_2O, CO_2, CO, and organics and gas phase CO. There are weak emission features present at 3.46, 3.39, and 3.54 μm that may be due to C-H stretch features in hydrogenated amorphous carbon (HAC) molecules as discussed in Grishko & Duley (2000) or aliphatic sidegroups on PAHs as discussed by de Muizon, d'Hendecourt, & Geballe (1990).

4.22. *NGC 7538 IRS 9*

NGC 7538 IRS 9 is a highly embedded, compact, luminous (4×10^4 $L_\odot$) infrared source located 2.7 kpc away (Werner et al. 1979). CO $J = 1-0$ and $J = 3-2$ studies indicate discontinuous and distinct outflow events, including a bipolar high-velocity outflow and a more recent extremely high-velocity outflow (Mitchell & Hasegawa 1991). The infrared spectrum exhibits strong absorptions of H_2O-ice. It has a 4.62 μm XCN feature weaker than that found in W33 A or RAFGL 7009S but stronger than in other sources, as well as the first detection and one of the highest abundances of NH_3-ice found to date (Lacy et al. 1998).

5. DISCUSSION

Much has been learned in the past several years about interstellar ices, as a direct result of the *ISO* mission, but many questions still remain. Our fits of laboratory data to observed spectra provide illustration of this. The fits include all ices with positive identifications and well-constrained abundances. We added contributions of H_2O, CH_3OH, CH_4, OCS, CO_2, $^{13}CO_2$, CO, XCN, SO_2, and NH_3 in abundances appropriate for each source, as discussed in § 3. It is immediately obvious from inspection of the relevant spectra in Figure 1 that there are regions in which the fit is satisfactory, but also regions containing absorptions that are unaccounted for. Note that beyond 8 μm the spectra are generally dominated by the 9.7 and 19 μm silicate features (not included in our fits), upon which weaker ice features (H_2O, CO_2, CH_3OH, etc.) are superposed.

5.1. *Interstellar Ices*

Here we give a brief overview of the principal components of interstellar ices with firm or probable identifications in our spectra. The column densities and mixing ratios (or upper limits where appropriate) for each molecule is given for each source in Tables 4–26. Parentheses indicate the uncertainties, while values given in square brackets indicate that the value was derived from another feature within the spectrum. For example, the optical depth of the 13 μm libration mode of water was determined from the fit to the 3 μm feature. See the table notes for details.

5.1.1. *Water*

Water is the most abundant and least volatile of the common ice species along lines of sight through dark molecular cloud material. The SWS covered the 3.05 μm O—H stretch mode, 4.5 μm combination mode, 6.0 μm H—O—H bending mode, and the 13 μm libration mode, the latter blended with the 9.7 μm silicate feature. In addition, the 45 μm transverse optical

TABLE 12
AFGL 989 Spectral Features

λ (μm)	FWHM (cm^{-1})	τ	Species	N (10^{17} cm^{-2})	$N/N(H_2O$ *100)	Reference
3.0	335	1.43(0.04)	H_2O	24(1)	100	1
3.25	62	0.069	PAH	...	...	2
3.46	51	0.050	HAC	...	...	3
	115	0.069	PAH	20	...	2
3.54	70	0.055(0.006)	CH_3OH	5.6(0.6)	23(2.5)	3
3.95	25	0.008(0.004)	CH_3OH	0.4(0.2)	1.7(0.9)	3
4.27	12.8	3.95	CO_2	8.1(0.1)	34(3)	1
		1.92	(Polar)	4.43	18.5	1
		2.03	(Nonpolar)	3.73	15.5	1
4.38	10	0.046(0.008)	$^{13}CO_2$	0.062(0.009)	0.26(0.05)	4
4.5[a]	700	[0.034]	H_2O	[24]	[100]	3
4.62[b]	29	0.022	XCN	0.07	0.3	
4.67	7.64	0.52(0.02)	CO	4.48(0.2)	18.7(0.7)	3
		0.23	(Polar)	3.25	13.5	3
		0.24	(Nonpolar)	1.23	5.1	3
4.91	23	0.024	OCS	0.02	0.08	5
5.83	32	0.06(0.02)	H_2CO	0.56(0.22)	2.3(1.0)	3
5.85	65		HCOOH	0.16(0.22)	0.7(1.0)	3
6.02[a]	185	[0.10]	H_2O	[24]	[100]	3
6.0	400	0.07(0.02)	Organic residue	...	...	3
6.85	88	0.09(0.02)	Organics/NH_4^+	...	...	3
7.282	18	0.016(0.01)	HCOOH	1.2(0.8)	5(3)	3
			$HCOO^-$	0.38(0.24)	1.6(1.0)	3
7.414	17.8	<0.016	$HCOO^-$	<0.18	<0.7	3
	10.6	<0.016	CH_3HCO	<1.2	<5	3
7.676	9	0.036(0.01)	CH_4	0.46(0.13)	1.9(0.5)	3
9.0	68	0.021(0.007)	NH_3	1.1(0.32)	4.6(1.3)	6
9.7	251	0.72(0.02)	Silicate	...	...	3
9.75	29	0.035	CH_3OH	0.60	2.5	3
13.3[a]	240	[0.30]	H_2O	[24]	[100]	3
15.2	21.5	0.35(0.01)	CO_2	9.6(0.4)	40(1.7)	3
18	156	0.21(0.02)	Silicate	...	...	3

Note.—Emission lines are present at 2.626 μm (Brβ), and 4.052 μm (Brα).
[a] Calculated from 3 μm feature.
[b] Gas phase CO?
References.—(1) Nummelin et al. 2001; (2) Bregman & Temi 2001; (3) this work; (4) Boogert et al. 2000; (5) Palumbo et al. 1997; (6) Gibb et al. 2001.

vibrational band of water has been detected in SWS/LWS spectra of several sources (Dartois et al. 1998). Our laboratory fits over- or underestimated the strength of the 13 μm feature in some lines of sight by up to 20%; we attribute this to uncertainty in the continuum since there are no true continuum points between 5.5 and 30 μm. The 3 and 6 μm features give discrepant column densities in several sources, with the 6 μm value systematically higher by a factor of up to 4 compared with that derived using the 3 μm feature (Keane et al. 2001c; Gibb et al. 2000). We argue (§ 5.2.2 below) that this is most likely caused by blending with the absorption of another species. Note that a good understanding of the 6 μm feature will be of vital importance for interpretation of *SIRTF* data, where the 3 μm region will be unavailable.

5.1.2. CO *and* CO_2

CO absorbs via its 4.67 μm fundamental vibrational band. The profile consists of a broad (polar) component peaking at 4.682 μm and a narrow (nonpolar) component peaking at 4.673 μm (Chiar et al. 1995, 1998). Typically, quiescent regions are dominated by pure CO or CO in a nonpolar mixture (Chiar et al. 1994, 1995). YSOs show evidence for warm ices or irradiation, and in exceptionally warm environments, the CO is found primarily in the gas phase. In addition, Boogert, Blake, & Tielens (2002) have reported a detection of the ^{13}CO ice feature at 4.78 μm in NGC 7538 IRS 9.

CO_2 has two strong bands: the ν_3 4.27 μm asymmetric stretching mode and the 15.2 μm ν_2 bending mode in addition to the weaker CO_2 overtone/combination band (reported in S140 by Keane et al. 2001a). CO_2 was first detected via the 15.2 μm feature using *IRAS* LRS (low-resolution spectrograph) by d'Hendecourt & Muizon (1989). These features were studied in detail in high-mass YSOs by Gerakines et al. (1999) and in low- or intermediate-mass YSOs by Nummelin et al. (2001). They found that generally CO_2/H_2O $\sim 17 \pm 3\%$ with the exception of two unusual sources, AFGL 989 and Elias 18, which exhibit very high (34%–37%) CO_2 concentrations. We also see evidence of comparably high concentrations of CO_2 in RCrA IRS 1 and RCrA IRS 2 and possibly Elias 1, though the signal-to-noise ratio for the latter is poor. The similarly high concentrations of CO_2 relative to H_2O observed toward field stars and low-mass YSOs indicates that CO_2 is formed efficiently without processing by an embedded source (Whittet et al. 1998). The 4.38 μm asymmetric stretching mode of $^{13}CO_2$ was studied in low- and high-mass YSOs, quiescent molecular cloud, and Galactic center sources

TABLE 13
AFGL 2136 Spectral Features

λ (μm)	FWHM (cm^{-1})	τ	Species	N (10^{17} cm^{-2})	$N/N(H_2O)$ *100	Reference
3.0	356	3.24(0.09)	H_2O	51	100	1
3.471	99.6	0.137(0.020)	HAC	...	...	2
3.54	29	0.060(0.010)	CH_3OH	2.6(0.4)	5.1(0.8)	2
3.95	115.3	<0.02	CH_3OH	<4.5	<8.9	3
4.27	18.5	2.40(0.08)	CO_2	7.8(0.3)	15.3(0.6)	4
4.38	10	0.071(0.008)	$^{13}CO_2$	0.073(0.005)	0.14(0.01)	5
4.5[a]	700	[0.07]	H_2O	[51]	[100]	
4.62	28	0.11(0.01)	XCN	0.66(0.06)	1.3(0.1)	3
4.67	7.64	0.24(0.01)	CO	2.68(0.25)	5.25(0.48)	3
			(Polar)	2.68	5.25	3
			(Nonpolar)	<0.1	<0.2	3
4.91	23	0.030(0.007)	OCS	0.43((0.01)	0.85(0.02)	3
5.83	47	0.08(0.03)	H_2CO	0.8(0.3)	1.6(0.6)	3
5.85	65		HCOOH	0.75(0.3)	1.5(0.6)	3
6.02[a]	136	0.23(0.04)	H_2O	51(9)	[100]	
6.0		<0.04	Organic residue	...	...	3
6.2	64	0.06(0.02)	?	...	...	3
6.85	80	0.18(0.02)	Organics/NH_4^+	...	...	3
7.243	16.8	<0.04	HCOOH	<2.8	<5.4	3
	19.8		CH_3HCO	<1.1	<2.1	3
7.414	17.8	<0.03	$HCOO^-$	<0.33	<0.66	3
	10.6		CH_3HCO	<2.3	<4.4	3
7.676	10.4	0.04(0.01)	CH_4	0.58(0.15)	1.1(0.3)	3
9.0	68	<0.021	NH_3	<1.1	<2.2	1
9.7	260	2.1(0.1)	Silicate	...	...	3
9.75	25	0.20(0.05)	CH_3OH	3.0(0.8)	5.9(1.5)	3, 6
13.3[a]	240	[0.46]	H_2O	[51]	[100]	
15.2	24.5	0.30(0.01)	CO_2	7.8(0.3)	15.3(0.6)	4
			(Polar)	6.2	12.2	4
			(Nonpolar)	1.6	3.1	4
18	185	0.72	Silicate	...	...	3

[a] Calculated from 3 μm feature.

References.—(1) Gibb et al. 2001; (2) Brooke et al. 1999; (3) this work; (4) Gerakines et al. 1999; (5) Boogert et al. 2000; (6) Skinner et al. 1992.

by Boogert et al. (2000) and gave consistent results with the CO_2 studies.

5.1.3. CH_3OH

CH_3OH has features at 3.53, 3.95, 6.8, and 9.75 μm. W33 A and RAFGL 7009S both have strong CH_3OH absorptions consistent with 15% and 30%, respectively, relative to H_2O (Dartois et al. 1999). In both cases the profile shape is consistent with a combination of pure CH_3OH and a $H_2O:CH_3OH$ mix. In most other sources, including any low-mass star-forming regions or dark molecular clouds, methanol is found to be a minor constituent, usually consistent with 5% or less. Recently, Pontoppidan et al. (2003), in a study of 40 low-mass protostars, found three sources with high (15%–25%) methanol abundances. CH_3OH is thought to form via H atom addition on a grain surface ($CO \rightarrow HCO \rightarrow H_2CO \rightarrow CH_3OH$), but laboratory experiments to confirm this formation route give discrepant results (Hiraoka et al. 2002; Watanabe & Kouchi 2002).

5.1.4. CH_4

CH_4-ice has been detected via its ν_4 deformation-mode feature at 7.67 μm in several sources at the 1%–2% level (Boogert et al. 1996), though AFGL 7009S is consistent with $\sim$4% (d'Hendecourt et al. 1996, this work). The position and shape of the profile is consistent with the presence of methane in a polar matrix. The lack of a cold CH_4 gas component and a low gas : solid CH_4 ratio support the interpretation that methane formed via H atom addition to atomic carbon on the grain surface in the cold dense cloud phase when the atomic C abundance was low (Boogert et al. 1998).

5.1.5. NH_3

Ammonia has an N-H stretch at 2.96 μm, an N-H deformation mode at 6.15 μm, and an umbrella mode at 9.3 μm (which shifts to 9.0 μm when NH_3 is a minor constituent in a polar ice). In addition to these, mixing NH_3 and water produces a broad feature over the long-wavelength wing of the 3 μm water feature, arising from the formation of ammonium hydrate groups. Each of the principal vibrational modes of ammonia is blended with a much stronger absorption, i.e., with the water stretching and bending modes and the 9.7 μm silicate feature, and this greatly hinders detection and quantitative analysis. Nonetheless, several studies have investigated the 3 μm region to determine upper limits of ammonia abundance in various lines of sight (Smith et al. 1989; Whittet et al. 1996; Chiar et al. 2000; Dartois & d'Hendecourt 2001; Gibb et al. 2001; Dartois et al. 2002). The 9 μm region has also been extensively studied and detections or upper limits obtained (Lacy et al. 1998; Gibb

TABLE 14
ELIAS 29 SPECTRAL FEATURES

λ (μm)	FWHM (cm^{-1})	τ	Species	N (10^{17} cm^{-2})	$N/N(H_2O)$ *100	Reference
3.0	335	1.85(0.08)	H_2O	34(6)	100	1
3.25	74	<0.03	C-H stretch	...	...	2
	88	0.085	PAH	21	...	3
3.49	94.3	0.089(0.007)	HAC	...	...	2
	88	0.065	PAH	14	...	3
3.54	30	<0.036	CH_3OH	<1.5	<4.4	1
3.95	115.3	<0.023	CH_3OH	<5.3	<15.6	4
4.267	17.1	2.77(0.2)	CO_2	6.7(0.5)	19.7(1.5)	5
4.38	10	0.071(0.009)	$^{13}CO_2$	0.083(0.005)	0.24(0.01)	1
4.5[a]	700	[0.046]	H_2O	[34]	[100]	
4.62	28	<0.01	XCN	<0.067	<0.20	6
4.673	4.4	~0.33	CO	1.7(0.3)	5.0(0.88)	1
			(Polar)	~0.2	~0.6	1
			(Nonpolar)	~1.5	~4.4	1
4.91	23	<0.01	OCS	<0.015	<0.044	1
5.81	21	<0.03	H_2CO	<0.6	<1.8	1
5.85	65	<0.03	HCOOH	<0.3	<0.09	1
6.02[a]	130	[0.16]	H_2O	[34]	[100]	
6.0	127	0.08(0.02)	Organic residue	...	...	4
6.85	116	0.12(0.03)	Organics/NH_4^+	...	...	4
7.243	16.8	<0.004	HCOOH	<0.3	<0.88	1
	19.8		$HCOO^-$	<0.1	<0.34	4
7.414	17.8	<0.03	$HCOO^-$	<0.33	<0.98	4
	10.6		CH_3HCO	<2.3	<6.6	4
7.631	10	<0.02	SO_2	<0.06	<0.18	4
7.676	11	<0.03	CH_4	<0.5	<1.5	1
9.0	64	<0.05	NH_3	<2.5	<7.3	7
9.7	242	1.32(0.06)	Silicate	...	...	4
13.3[a]	240	[0.31]	H_2O	[34]	[100]	
15.2	23.1	0.33(0.02)	CO_2	6.7(0.5)	19.7(1.5)	5
			(Polar)	6.2	18.2	5
			(Nonpolar)	0.5	1.5	5
18	168	0.31(0.05)	Silicate	...	...	4

[a] Calculated from 3 μm feature.

REFERENCES.—(1) Boogert et al. 2000; (2) Brooke et al. 1999; (3) Bregman & Temi 2001; (4) this work; (5) Gerakines et al. 1999; (6) Whittet et al. 2001; (7) Gibb et al. 2001.

et al. 2001; Gürtler et al. 2002). Further constraints have recently been placed by a search for a weak feature at 2.21 μm (Taban et al. 2003), shortward of the wavelength range covered by *ISO*-SWS. It is interesting and surprising that a molecule predicted, on the basis of chemical models, to be abundant in the solid phase in cold interstellar clouds (Tielens & Hagen 1982) is found to have an upper limit of ~5% in most lines of sight. This may indicate subsequent processing either thermally or through energetic processing (Pendleton et al. 1999). These results are nevertheless consistent with NH_3 abundances in comets, which are typically ~1% (Bockelée-Morvan et al. 2000).

5.1.6. XCN

The absorption feature at 4.62 μm is, strictly speaking, unidentified, but it is attributed with some confidence to C ≡ N bond vibrations in an organic molecule, most probably a cyanate or the OCN^- ion (Whittet et al. 2001). The carrier is linked, through laboratory work, to energetic processing of ices by UV photons or ions, and the importance of the 4.62 μm feature is thus that it provides a diagnostic of such processing. Amongst our sources, W33 A and AFGL 7009S have the strongest 4.62 μm features, whilst several other massive YSOs show weaker absorption at this wavelength. The feature is very weak or absent in low-mass YSOs, many high-mass YSOs, dark clouds, and the diffuse ISM.

5.1.7. *Other Minor Constituents*

In addition to the species discussed above, there are additional absorptions at 5.83 and 5.85 μm attributable to HCOOH and H_2CO (Keane et al. 2001c). There are also weak features at 7.24 and 7.41 μm, which have not been uniquely identified but are consistent with the CH deformation mode of formic acid and either the formate ion ($HCOO^-$) or acetaldehyde (CH_3HCO), respectively (Schutte et al. 1999). Several sources (W33 A, NGC 7538 IRS 9, Mon R2 IRS 3) exhibit excess absorption at 6.0 μm (see below) that is not attributable to water or other known ice constituents. A weak, broad absorption feature seen at 6.2 μm may arise from absorption by polycyclic aromatic hydrocarbons (PAHs) (Keane et al. 2001c).

5.1.8. *Upper Limits on Amino Acids*

Amino acids have long been discussed as a possible constituent of interstellar matter. Previous searches have focused on the gas phase (see Snyder 1997 for a review), but recent work has emphasized the possibility that they might be a minor constituent of ices that have been subjected to UV

TABLE 15
Sgr A* Spectral Features

λ (μm)	FWHM (cm^{-1})	τ	Species	N (10^{17} cm^{-2})	$N/N(H_2O)$ *100	Reference
3.0	335	0.50(0.01)	H_2O	12.4(2.5)	100	1
3.28		<0.02	C-H stretch	...	...	1
3.46	80	0.21(0.01)	HAC	...	...	1
3.54	30	<0.01	CH_3OH	<0.5	<4	1
3.95	115.3	<0.001	CH_3OH	<0.4	<3	1
4.27	16.7	0.70(0.01)	CO_2	1.7(0.2)	13.7(1.6)	2
4.38	7.2	<0.07	$^{13}CO_2$	<0.12	<1	3
4.5[a]	700	[0.017]	H_2O	[12.4]	[100]	3
4.62	29	~0.14	XCN	~0.83	~6.7	4
4.67	7.64		CO	<1.5	<12	1
4.91	20	<0.03	OCS	<0.04	<0.3	3
5.81	21		H_2CO	<0.3	<2.4	1
6.02[a]	185	[0.07]	H_2O	[12.4]	[100]	3
6.0		<0.03	Organic residue	...	...	3
6.2	60	0.05(0.01)	?	...	...	1
6.85	88	0.05(0.01)	OrganicsNH_4^+	...	...	1
7.243	19	0.03(0.01)	HCOOH	0.8(0.2)	6.5(1.6)	1
7.676	10.4	0.017(0.003)	CH_4	0.30(0.07)	2.4(0.56)	1
9.0	68	<0.012	NH_3	<0.61	<4.9	5
9.7	176	2.31(0.02)	Silicate	...	...	3
13.3[a]	240	[0.11]	H_2O	[12.4]	[100]	3
15.2	20.3	0.077(0.005)	CO_2	1.7(0.2)	13.7(1.6)	2
			(Polar)	1.7	13.7	2
			(Nonpolar)	<0.1	<0.8	2
18	140	0.57(0.01)	Silicate	...	...	3

Note.—There are emission features at 2.62 μm (Brβ), 2.75 μm (Pfη), 2.87 μm (Pfζ), 3.03 μm (Pfϵ), 3.30 μm (Pfδ), 3.73 μm (Pfγ), 4.05 μm (Brα), 4.65 μm (Pfβ), 5.34 μm (Fe II, $^4F_{9/2}-^6D_{9/2}$?), 5.51 μm (H_2?), 5.91 μm (H I 9–6), 6.64 μm (Ni II $^2D_{3/2}-^2D_{5/2}$), 6.91 μm (H_2?), 6.98 μm (Ar II $^2P_{1/2}-^2P_{3/2}$), 7.35 μm (?), 7.46 μm (Pfα), 7.50 μm (Ni I $^3F_3-^3F_4$?), 12.81 μm (Ne II $^2P_{1/2}-^2P_{3/2}$), 15.56 μm (Ne III $^3P_1-^3P_2$), 18.71 μm (S III $^3P_2-^3P_1$), 22.93 μm (Fe III $^5D_3-^5D_4$), 25.91 μm (O IV $^2P_{3/2}-^2P_{1/2}$), 33.04 μm (Fe III $^5D_2-^5D_3$), 33.48 μm (S III $^3P_1-^3P_0$), 34.81 μm (Si II $^2P_{3/2}-^2P_{1/2}$), 35.35 μm ($^6D_{5/2}-^6D_{7/2}$), and 36.01 μm (Ne III $^3P_1-^3P_0$).

[a] Calculated from 3 μm feature.

References.—(1) Chiar et al. 2000; (2) Gerakines et al. 1999; (3) this work; (4) Moneti et al. 2001; (5) Gibb et al. 2001.

photolysis (Bernstein et al. 2002; Munoz Caro et al. 2002; Woon 2002). The infrared vibrational spectra of amino acids exhibit several features that might in principle yield detections (e.g., Ehrenfreund et al. 2001), but quantitative analysis is inhibited by blending with other, far stronger, ice features in interstellar spectra, most notably those of H_2O.

The most prominent infrared feature in laboratory spectra of the simplest amino acid, glycine (NH_2CH_2COOH), is the C=O (carbonyl) stretch: in an Ar matrix at 12 K this is centered at ~5.62 μm, i.e., on the short-wavelength side of the 6.0 μm feature in astronomical spectra. Considering our spectrum of W33A, we set an approximate upper limit of $\tau_{5.62} < 0.05$ on any discrete feature at this wavelength. Assuming a band strength of $\sim 3 \times 10^{-17}$ cm per molecule (Ehrenfreund et al. 2001) and a width ~ 20 cm^{-1} (consistent with the Ar matrix isolation spectrum), we estimate an upper limit of 3×10^{16} cm^{-2} on the column density of glycine in this line of sight, which is ~0.3% of the H_2O column density. Note that if the feature is broadened, as expected for inclusion in a water-dominated matrix, the estimated limit will be less stringent.

5.2. *Unidentified Features*

5.2.1. *The* 3.2 – 3.8 μm *Wing*

In common with previously published results (see Smith et al. 1989), all of our sources for which fits are presented exhibit a wing on the long-wavelength side of the 3.1 μm O—H stretch H_2O-ice profile. Whilst there are constituents in our mixtures—NH_3 (ammonium hydrate), CH_3OH, and CH_4—that contribute to absorption in this spectral region, their abundance is insufficient to account for the wing. Other possibilities include organic residues that contribute C—H stretching absorptions at ~3.4 μm, and scattering. However, a substantial contribution by organic refractories can be excluded for some sources by the weakness or absence of associated absorption in the 6 μm region (see below); even in cases where this is thought to be present, the implied contribution at 3.4 μm is generally small (Gibb & Whittet 2002). Similarly, attempts to account for the wing quantitatively in terms of scattering by large core-mantle grains have met with only limited success (see review by Whittet 2003). The long-wavelength wing continues to defy an explanation.

5.2.2. *Features Overlapping the* 6.0 μm H_2O *Bending Mode*

There has been much discussion in the literature concerning the H_2O column density toward W33 A and other sources (Gibb et al. 2000; Keane et al. 2001c). We demonstrate in Figure 1*o* and Table 18 that one can simultaneously fit the 3, 4.5, and 13 μm optical depths in W33 A with an H_2O column density of 1.1×10^{19} cm^{-2}, whereas fitting the 6 μm bending-mode feature independently results in a much higher column density. This discrepancy is greatest in W33 A but also present to a lesser extent in several other sources (Keane et al. 2001c).

TABLE 16
GCS 4 Spectral Features

λ (μm)	FWHM (cm^{-1})	τ	Species	N (10^{17} cm^{-2})	$N/N(H_2O)$ *100	Reference
3.0	335	0.16(0.01)	H_2O	3.0(0.3)	100	1
3.28	25	<0.05	...	...	...	1
3.40	80	0.15(0.01)	...	...	...	1
4.27	12.8	0.22(0.02)	CO_2	0.7(0.2)	23.3(6.7)	2
4.5[a]	700	[0.004]	H_2O	[3.0]	[100]	
4.62	28	<0.04	XCN	<0.24	<8	3
4.67	7.64		CO	<0.9	<30	4
4.91	19.6	<0.02	OCS	<0.02	<0.8	3
6.02[a]	185	[0.013]	H_2O	[3.0]	[100]	
6.2	60	0.08(0.02)	C-C stretch	...	...	1
6.85	88	<0.03	Organics/NH_4^+	...	...	1
7.243	19	<0.03	HCOOH	<2	<67	3
7.676	10.4	<0.03	CH_4	<0.5	<17	1
9.0	68	<0.030	NH_3	<1.6	<53	5
9.7	197	2.8(0.3)	Silicate	...	...	3
13.3[a]	240	[0.033]	H_2O	[3.0]	[100]	
15.2	19	0.05(0.01)	CO_2	0.7(0.2)	23.3(6.7)	2
			(Polar)	0.5	16.7	2
			(Nonpolar)	<0.2	<6.7	2
17.4	113	0.42(0.1)	Silicate	...	...	3

Note.—There are emission features at 4.05 μm (Br α), 6.99 μm (Ar II, $^2P_{1/2}$—$^2P_{3/2}$), 12.81 μm (Ne II, $^2P_{1/2}$—$^2P_{3/2}$), 15.56 μm (Ne III, $^3P_1$—$^3P_2$), 18.72 μm (S III, $^3P_2$—$^3P_1$), 22.94 μm (Fe III, $^5D_3$—$^5D_4$), 33.49 μm (S III, $^3P_1$—$^3P_0$), 34.81 μm (Si II, $^2P_{3/2}$—$^2P_{1/2}$), and 36.03 μm (Ne III, $^3P_0$—$^3P_1$).

[a] Calculated from 3 μm feature.

References.—(1) Chiar et al. 2000; (2) Gerakines et al. 1999; (3) this work; (4) Chiar et al. 1998; (5) Gibb et al. 2001.

While it has been argued that the difference might be due to scattering, the fact that the 13 μm libration mode is also consistent with the fit at 3 and 4.5 μm and not consistent with a column density more than 3 times greater argues against this explanation, at least in W33 A and AFGL 7009S. This lends support to the conclusion reached by Gibb & Whittet (2002) that a substantial amount of the 6 μm absorption can be attributed to some component other than water in both W33 A and AFGL 7009S.

The residual after subtracting the water component from the 6 μm profile in W33 A and AFGL 7009S is well fitted by a refractory organic residue. Examples of appropriate residues include those synthesized by exposure of simple ices to UV radiation (Greenberg et al. 1995) and organic material extracted from the Murchison meteorite. An organic refractory component has been added to the ices for these sources in Figure 1, to illustrate the improvement in fit. Additional weak features remain at 5.8 and 6.2 μm, possibly caused by an ice component with a C=O stretch (such as HCOOH or H_2CO) and by PAH absorption, respectively. There is also evidence of an organic refractory component in Mon R2 IRS 3 and NGC 7538 IRS 9 (Gibb & Whittet 2002). Other sources, such as S140, W3 IRS 5, and Elias 29 do not require any organic residue to account for the 6 μm feature. Even those sources that do not exhibit excess absorption at 6 μm, show evidence for other minor constituents at 5.85 and 6.2 μm.

If organic refractory matter is responsible for excess absorption at 6 μm, a correlation with the 4.62 μm XCN feature may be expected (§ 5.1.6). This is indeed the case, as shown in Figure 2*a*. The correlation is dominated by two sources (W33 A and AFGL 7009S) that have deep 4.62 μm absorption and relatively deep 6 μm excesses. However, there are some sources with no measurable 6 μm excess that exhibit weak XCN absorption, and conversely, so the correspondence is not perfect. It may be that similar conditions are needed to synthesize XCN and the carrier of the 6 μm excess, but they are not one and the same.

5.2.3. *The* 6.8 μm *Feature*

Another persistent problem is the identification of the 6.8 μm feature. This feature has not been satisfactorily explained by any available laboratory comparison spectrum. A small percent of the area of the feature may be filled by contributions from ices such as CH_3OH and CH_3CHO, but most of the feature cannot be explained by known ice constituents. Identification is complicated by the fact that the peak position and profile change from one source to another. Keane et al. (2001c) interpreted the absorption to be due to the superposition of two components, C1 and C2, with different peak positions. Schutte & Khanna (2003) discuss NH_4^+ as a possible candidate. This molecule is easily produced in the laboratory by processing of interstellar ice analogs and exhibits an increase in peak position with increasing temperature. While their spectra were not perfect matches to the interstellar bands, the similarity is certainly suggestive and should be further investigated.

With the larger database of sources in this study, we investigated correlations of the 6.8 μm feature with water (via the 3 μm feature), the excess absorption at 6 μm, and the 4.62 μm XCN feature. Figure 2 shows the results of these correlations. The pluses and diamonds indicate sources for which the 6.8 μm feature peaks at lower and higher wavelength, respectively (C1 and C2 in Keane et al. 2001c, or the low- and high-temperature components of NH_4^+ of Schutte & Khanna 2003). The circles denote sources with weak and noisy 6.8 μm features. The optical depths at 6.8 μm were derived after subtraction of the 6 μm water wing and CH_3OH when appropriate.

TABLE 17
GCS 3I Spectral Features

λ (μm)	FWHM (cm^{-1})	τ	Species	N (10^{17} cm^{-2})	$N/N(H_2O)$ *100	Reference
3.0	335	0.23(0.02)	H_2O	4.7(0.4)	100	1
3.28	25	0.026(0.005)	Aromatic HC	...	...	1
3.40	93	0.16(0.01)	HAC	...	...	1
3.48	36	0.09	HAC	...	...	2
3.54[a]	30	<0.03	CH_3OH	<1.3	<27	2
3.95	115.3	<0.01	CH_3OH	<2.3	<49	2
4.27	15.4	0.48(0.02)	CO_2	1.1(0.1)	23.4(2.1)	3
			(Polar)	1.1	23.4	3
			(Nonpolar)	<0.1	<2.1	3
4.38	4	0.042(0.015)	$^{13}CO_2$	0.021(0.004)	0.45(0.08)	4
4.5[b]	700	[0.006]	H_2O	[4.7]	[100]	2
4.62[c]	28	<0.05	XCN	<0.30	<6.3	2
4.67	7.64	<0.1	CO	<0.9	<19	5
4.91	19.6	<0.04	OCS	<0.05	<1.0	2
6.02[b]	185	[0.021]	H_2O	[4.7]	[100]	2
6.2	34	0.10(0.02)	C-C stretch	...	...	1
6.85	88	0.04(0.01)	Organics/NH_4^+	...	...	1
7.243	16.8	<0.03	HCOOH	<2.7	<57	1
	19.8		$HCOO^-$	<0.88	<19	1
7.414	17.8	<0.03	$HCOO^-$	<0.33	<7.1	2
	10.6		CH_3HCO	<2.2	<48	2
7.676	10.4	<0.02	CH_4	<0.3	<6.4	1
9.0	68	<0.034	NH_3	<1.8	<38	6
9.7	224	2.38	Silicate	...	...	7
13.3[b]	240	[0.05]	H_2O	[4.7]	[100]	2
18	211	1.32(0.04)	Silicate	...	...	2

Note.—There are emission features at 6.986 μm (Ar II $^2P_{1/2}-^2P_{3/2}$), 12.815 μm (Ne II $^2P_{1/2}-^2P_{3/2}$), 18.718 μm (S III $^2P_2-^3P_1$), 33.48 μm (S III $^3P_1-^3P_0$), and 34.81 μm (Si II $^2P_{3/2}-^2P_{1/2}$).

[a] Blended with HAC.

[b] Calculated from 3 μm feature.

[c] Gas phase CO.

References.—(1) Chiar et al. 2000; (2) this work; (3) Gerakines et al. 1999; (4) Boogert et al. 2000; (5) Chiar et al. 1998; (6) Gibb et al. 2001; (7) Schutte et al. 1998.

Figure 2*b* shows the optical depth at 3 μm versus that of the 6.8 μm feature. While both features increase in optical depth, there is not a single line correlation. Rather, there is a group of five objects (Mon R2 IRS 3, NGC 7538 IRS 1, Orion BN, Orion IRc2, and Mon R2 IRS 2) that have much stronger 6.8 μm features (by a factor of 2 or more) than other sources of comparable water column density. For example, Mon R2 IRS 3 and S140 have the same water column densities and similar profiles, both exhibiting evidence of annealing of the 3 μm water band. Yet S140 has a 6.8 μm feature that is 2.6 times weaker than that of Mon R2 IRS 3. Both sources peak at the same position, with similar profiles that indicate dominance by the long-wavelength (or higher temperature in the case of NH_4^+) component, so temperature alone cannot apparently account for the abundance variation. While all five sources that have the higher 6.8 μm absorption are high-mass objects, the remaining sources are a mix of high-, low-, and intermediate-mass objects. The correlation of optical depths is also independent of the temperature of ice along the line of sight as indicated by annealing of the 3 μm H_2O or 15.2 μm CO_2 features or peak position of the 6.8 μm feature and could indicate, for example, different starting abundances of the molecule(s) giving rise to the feature.

We also investigated the correlation of the 6.8 μm feature with that at 4.62 μm (Fig. 2*c*). OCN^- and NH_4^+ are both formed under similar laboratory conditions. With the possible exception of Orion IRc2 (which has gas phase CO at 4.62 μm superposed on an underlying weak feature we attribute to XCN), all the sources dominated by the long-wavelength component (*diamonds*) are lacking XCN. If the XCN carrier is OCN^-, which is stable in a vacuum to more than 200 K (Hudson, Moore, & Gerakines 2001), and if the long-wavelength component is due to hot NH_4^+ (180–240 K), as suggested by Schutte & Khanna (2003), then a weak XCN feature for the sources represented by diamonds in Figure 2*c* may be an indication of temperatures exceeding ~200 K in regions where these ions are formed. The sources with the shorter wavelength C1 component (fit by the cooler NH_4^+ spectra) generally exhibit increasing XCN with increasing optical depth of the 6.8 μm feature. Sources such as Mon R2 IRS 3 and NGC 7538 IRS 9 have very similar 6.8 μm optical depths but peak at different positions. NGC 7538 IRS 9 has a substantial XCN feature, while the "warmer" Mon R2 IRS 3 does not. Hence, the 4.62 μm feature is not inconsistent with the interpretation of NH_4^+ as the principle carrier of the 6.8 μm feature.

One concern with this interpretation is that OCN^- provides an inadequate source for negative counterions to balance the positively charged NH_4^+, and no other negative ions have been conclusively identified. Schutte & Khanna (2003) discuss how these counterions were only apparent after sublimation of water ice in their laboratory experiments. Nevertheless, without firm upper limits or a conclusive detection of other negatively charged ice species, this remains a concern for identification of the 6.8 μm absorption. Another reason for

TABLE 18
W33A Spectral Features

λ (μm)	FWHM (cm^{-1})	τ	Species	N (10^{17} cm^{-2})	$N/N(H_2O)$ *100	Reference
3.0	335	5.5(1.5)	H_2O	110(30)	100	1
3.477	80.7	0.290(0.040)	HAC	...	...	2
3.53	29	0.27(0.05)	CH_3OH(pure)	11.9(2.2)	10.8(2.0)	2
	29	0.07(0.02)	Polar	2.7(0.8)	2.5(0.7)	2
3.95	115.3	0.5	CH_3OH	18.5	16.8	3
4.27	20	>5	CO_2	14.5(1.3)	13.2(1.2)	4
			(Polar)	12.3	11.2	4
			(Nonpolar)	2.2	2.0	4
4.38	9.5	0.225(0.015)	$^{13}CO_2$	0.274(0.021)	0.249(0.019)	5
4.5	700	0.1(0.05)	H_2O	70(40)	64(36)	1
4.62	24.7	1.3	XCN	6.9	6.3	6, 7
4.67	7.64	1.30(0.05)	CO	8.9(0.5)	8.1(0.5)	8
		0.68(0.05)	(Polar)	6.6(0.5)	6.0(0.5)	8
		0.79(0.05)	(Nonpolar)	2.3(0.2)	2.1(0.2)	8
4.78	15	<0.02	^{13}CO	<0.25	<0.23	9
4.91	23	0.14	OCS	0.2	0.2	10
5.81	21	0.14(0.07)	H_2CO	3.45(1.7)	3.1(1.6)	9
5.85	65	0.32(0.07)	HCOOH	4.12(0.9)	3.7(0.8)	9
6.02	172	0.49(0.07)	H_2O	110	100	11
6.0	420	1.12(0.07)	Organic residue	...	...	11
6.2	60	0.22(0.07)	PAH?	?	?	11
6.85	79	1.07(0.07)	Organics/NH_4^+	...	...	11
7.243	19	0.10(0.02)	HCOOH	7.8	7.1	12
			$HCONH_2$	6.3	5.7	12
7.414	15	0.10(0.03)	$HCOO^-$	0.93	0.85	12
			CH_3HCO	10.8	9.82	12
7.631	27.7	0.082(0.005)	SO_2	1.74(0.90)	1.58(0.82)	13
7.676	10.4	0.120(0.005)	CH_4	1.7(0.2)	1.5(0.2)	13
8.90	34	0.1	CH_3OH	15	14	1
9.0	68	0.45(0.10)	NH_3	17(4)	15(4)	1
9.7	295	7.84(0.12)	Silicate	...	...	14
9.75	30	0.9(0.2)	CH_3OH	15(4)	14(4)	1
13.3[a]	240	[1.2]	H_2O	[110]	[100]	9
15.24	27.4	0.58(0.01)	CO_2	14.5(1.3)	13.2(1.2)	4
			(Polar)	12.3	11.2	4
			(Nonpolar)	2.2	2.0	4
18	200	1.20(0.02)	Silicate	...	...	9

Note.—Emission features are present at 3.8195 μm (H I 16–6), 3.9075 μm (H I 15–5), and 4.0523 μm (Brα).
[a] Calculated based on 3 μm feature.
References.—(1) Gibb et al. 2000; (2) Brooke et al. 1999; (3) Dartois et al. 1999; (4) Gerakines et al. 1999; (5) Boogert et al. 2000; (6) Whittet et al. 2001; (7) Demyk et al. 1998; (8) Chiar et al. 1998; (9) this work; (10) Palumbo et al. 1997; (11) Gibb & Whittet 2002; (12) Schutte et al. 1999; (13) Boogert et al. 1996; (14) Willner et al. 1982.

concern is the apparent lack of NH_3 in interstellar ices along these lines of sight. NH_3 is needed in laboratory studies to produce NH_4^+ and the work of Hudson et al. (2001) indicates that OCN^- originates in a polar mantle from irradiation of an NH_3 mixture. In most lines of sight, the NH_3 abundance is inferred to be less than 5%. Analysis of the 9 μm region in W33 A and NGC 7538 IRS 9 indicates abundances of $\sim$10%–15%, in contradiction to the results of Taban et al. (2003) for W33 A, who infer an upper limit of 5%. More work must be done to answer this question of the nitrogen component of interstellar ices. An alternative explanation is that the 6.8 μm feature can be attributed to two independent carriers and that XCN is correlated with C1 but not with C2 of the 6.8 μm feature. We are unable to distinguish between these two interpretations at the current time.

If the 6 μm excess is due at least in part to NH_4^+ as suggested by Schutte & Khanna (2003) then it would correlate with the 6.8 μm feature (see Fig. 2*d*). What is found is that for sources with comparable contributions from both C1 and C2 as per Keane et al. (2001c) (denoted by plus signs in Fig. 2), increasing optical depth at 6.8 μm generally corresponds to an increase in the 6 μm excess. The sources lacking a 6 μm excess are more problematic. It is unclear how two sources with very similar 6.8 μm profile shapes and optical depths, such as W3 IRS 5 and Orion BN, can have more than a factor of 4 difference in the 6 μm excess if both features are due to the same absorber. Perhaps some fraction of the excess at 6 μm could be due to NH_4^+, the remainder being due to a different species, such as an organic refractory component as suggested by Gibb & Whittet (2002).

5.3. *Overall Ice Composition*

Previous studies (e.g., Gibb et al. 2000) have discussed an evolutionary sequence for ice mantle compositions in varying lines of sight. In general, increased processing leads to sub-

TABLE 19
AFGL 7009S Spectral Features

λ (μm)	FWHM (cm^{-1})	τ	Species	N (10^{17} cm^{-2})	$N/N(H_2O)$ *100	Reference
3.0[a]	335	...	H_2O	...	...	
3.95	115.3	0.09	CH_3OH	35.5	32.3	1
4.27[a]	12.8		CO_2			
4.38	7.2		$^{13}CO_2$	0.4	0.36	2
4.5	700	[0.15]	H_2O	[110]	[100]	2
4.62	32	0.65	XCN	4.2	3.8	3, 4
4.67	7.64		CO	18	16.4	2
4.89	27.3	0.065(0.033)	OCS	0.11(0.06)	0.10(0.05)	5
5.83	47	0.56(0.06)	H_2CO	3.3(0.61)	3.0(0.56)	6
6.02	150	1.2(0.1)	H_2O	110	100	2
6.0		0.53(0.06)	Organic residue	...	...	6
6.2	58	0.10(0.06)	?	...	...	6
6.85	85	0.93(0.06)	Organics/NH_4^+	...	...	6
7.243	12.5	0.11(0.02)	HCOOH	5.2(1.1)	4.7(1.0)	5
			$HCOO^-$	1.7(0.4)	1.5(0.4)	5
7.414	14.1	0.09(0.02)	$HCOO^-$	0.79(0.16)	0.72(0.15)	5
			CH_3HCO	9.0(1.8)	8.2(1.6)	5
7.676	10.4	~0.3	CH_4	4.3	3.9	2
9.0	68	~0.5(0.2)	NH_3	~19(8)	17.3(7.3)	7
9.7	308	4.0(0.3)	Silicate	...	...	5
13.3	240	1.2	H_2O	110	100	2
15.2	27.4		CO_2	25	22.7	2
18	184	2.3(0.1)	Silicate	...	...	5

[a] Saturated.

References.—(1) Dartois et al. 1999; (2) d'Hendecourt et al. 1996; (3) Whittet et al. 2001; (4) Demyk et al. 1998; (5) this work; (6) Gibb & Whittet 2002; (7) Gibb et al. 2001.

limation of more volatile species and production of more complex species, such as XCN and CH_3OH. This sequence is for the most part supported by the current study with some minor differences.

Table 27 gives a concise comparison of compositions in varying lines of sight, according to the gross properties of the environment (mass of YSOs and evidence of strong or weak processing). Typically, cool quiescent regions that have not undergone significant processing of the icy mantle material start with a polar (H_2O, CO_2, NH_3? bearing) mantle coated by a CO rich apolar mantle. Only upper limits for CH_3OH, XCN, and NH_3 have been determined in these regions using *ISO* data. Low-mass star formation regions show a similar composition to the quiescent dark molecular cloud medium, indicating that little processing has occurred along much of the line of sight. CO_2 and CO are found primarily in the polar and apolar mantles, respectively, in both environments, and this trend has been consistently observed in several lines of sight.

TABLE 20
R CrA IRS 2 Spectral Features

λ (μm)	FWHM (cm^{-1})	τ	Species	N (10^{17} cm^{-2})	$N/N(H_2O)$ *100	Reference
3.0	335	1.14(0.07)	H_2O	22.8	100	1
3.472	77	0.041(0.011)	HAC	...	...	2
3.54	30	<0.19	CH_3OH	<8	<35	1
3.95	115.3	<0.044	CH_3OH	<10.4	<46	1
4.27[a]	14	[3.1]	CO_2	[8.3]	[36]	1
4.38	7	0.13(0.02)	$^{13}CO_2$	0.117(0.009)	0.513(0.04)	3
4.5[b]	700	[0.031]	H_2O	[22.8]	[100]	
4.62	28	<0.015	XCN	<0.084	<0.37	4
4.67	3.22	4(1)	CO	12(3)	53(13)	5
		0.01(0.01)	(Polar)	0.6(0.7)	2.6(3.1)	5
		4(1)	(Nonpolar)	11(3)	48(13)	5
4.91	23	<0.22	OCS	<0.32	<1.4	1
15.2	18.8	0.44(0.03)	CO_2	8.3(1.2)	36(5)	1
			(Polar)	5.4	24	1
			(Apolar)	3.2	14	1

[a] Saturated.

[b] Calculated based on 3 μm feature.

References.—(1) This work; (2) Brooke et al. 1999; (3) Boogert et al. 2000; (4) Whittet et al. 2001; (5) Chiar et al. 1998.

TABLE 21

RCrA IRS 1 (HH 100 IR) Spectral Features

λ (μm)	FWHM (cm^{-1})	τ	Species	N (10^{17} cm^{-2})	$N/N(H_2O)$ *100	Reference
3.0.....	335	1.44(0.06)	H_2O	24(1)	100	1
3.25.....	57	0.032(0.010)	C-H stretch	...	...	2
3.469.....	103	0.041(0.005)	HAC	...	...	2
3.54.....	30	<0.09	CH_3OH	<3.8	<15	3
4.27[a].....	12.8	~2.3	CO_2	~7.2	~30	3, 4
4.38.....	10	<0.14	$^{13}CO_2$	<0.25	<0.95	3
4.5[b].....	700	[0.032]	H_2O	[24]	[100]	3
4.62.....	29	<0.05	XCN	<0.30	<1.2	5
4.67.....	3.67	1.55(0.05)	CO	6.5(0.6)	27(2.5)	6
		0.21(0.05)	(Polar)	2.5(0.6)	10.4(2.5)	6
		1.40(0.05)	(Nonpolar)	4.1(0.2)	17.1(0.8)	6
4.91.....	25	0.066(0.038)	OCS	0.10(0.06)	0.42(0.25)	3
6.02[b].....	185	[0.089]	H_2O	[24]	[100]	3
6.0.....	65	0.1(0.06)	Organic residue	...	...	3
6.85.....	88	0.08(0.04)	Organics/NH_4^+	...	...	3
7.676.....	8.4	0.05(0.02)	CH_4	0.6(0.2)	2.6(1.0)	3
9.0.....	64	<0.06	NH_3	<3	<13	1
9.7.....	192	0.61(0.05)	Silicate	...	...	3
13.3[b].....	240	[0.21]	H_2O	[25.9]	[100]	3
15.2.....	22.4	0.40(0.02)	CO_2	7.2(0.6)	30(3)	3
18.....	175	0.20(0.04)	Silicate	...	...	3

[a] Saturated.

[b] Calculated based on 3 μm feature.

References.—(1) Whittet et al. 1996; (2) Brooke et al. 1999; (3) this work; (4) Nummelin et al. 2001; (5) Whittet et al. 2001; (6) Chiar et al. 1998.

TABLE 22

AFGL 2591 Spectral Features

λ (μm)	FWHM (cm^{-1})	τ	Species	N (10^{17} cm^{-2})	$N/N(H_2O)$ *100	Reference
3.0.....	407	0.74(0,02)	H_2O	12(0.3)	100	1
3.25.....	56	0.026	PAH	...	...	2
3.464.....	111.3	0.045(0.005)	HAC	...	...	3
			PAH?	...	...	2
3.54.....	30	0.039(0.007)	CH_3OH	1.7(0.3)	14(2)	4
3.95.....	115.3	<0.008	CH_3OH	<1.8	<14.8	4
4.27.....	24.0	0.55(0.01)	CO_2	1.6(0.2)	13.3(1.7)	4
4.38.....	7	0.034(0.005)	$^{13}CO_2$	0.026(0.003)	0.22(0.03)	6
4.5[a].....	700	[0.016]	H_2O	[12]	[100]	
4.62[b].....	29	...	XCN	...	...	
4.67[b].....	7.64	...	CO	...	...	
4.91.....	23	0.024	OCS	0.02	0.17	7
6.02[a].....	185	[0.041]	H_2O	[12]	[100]	
6.85.....	88	~0.04	Organics/NH_4^+	...	...	4
7.243.....	16.8	<0.03	HCOOH	<2.1	<17	4
	19.8	<0.03	CH_3HCO	<0.79	<6.6	4
7.414.....	17.8	<0.01	$HCOO^-$	<0.11	<0.93	4
	10.6	<0.01	CH_3HCO	<0.75	<6.2	4
7.676.....	10.4	<0.02	CH_4	<0.33	<2.7	4
9.0.....	68	<0.0051	NH_3	<0.27	<2.3	8
9.7.....	259	2.25	Silicate	...	...	4
13.3[a].....	240	[0.11]	H_2O	[12]	[100]	
15.2.....	25.1	0.073(0.005)	CO_2	1.6(0.2)	13.3(1.7)	5
			(Polar)	1.2	10	5
			(Nonpolar)	0.4	3.3	5
18.....	245	0.86	Silicate	...	...	4

Note.—There are gas phase absorption lines throughout the 5–8 μm region.

[a] Calculated from 3 μm feature.

[b] Gas phase CO.

References.—(1) Gibb et al. 2001; (2) Bregman & Temi 2001; (3) Brooke et al. 1999; (4) this work; (5) Gerakines et al. 1999; (6) Boogert et al. 2000; (7) Palumbo et al. 1997; (8) Gibb et al. 2000.

TABLE 23
CYGNUS OB2 12 SPECTRAL FEATURES

λ (μm)	FWHM (cm^{-1})	τ	Species	N (10^{17} cm^{-2})	Reference
3.0		<0.02	H_2O	<0.40	1
3.477	80.7	0.04(0.01)	HAC	...	2
4.27		<0.02	CO_2	<0.05	2
4.62	24.7	<0.015	XCN	<0.084	3
6.2	60	0.06(0.04)	?	...	2
6.85	79	<0.034	Organics/NH_4^+	...	4
9.7	320	0.54(0.06)	Silicate	15	2
10.0	20	<0.0067	HMT	<0.27	1

REFERENCES.—(1) Bowey et al. 1998; (2) Whittet et al. 1997; (3) Whittet et al. 2001; (4) this work.

However, a recent study by Pontoppidan et al. (2003) has reported large (~15%) abundances of CH_3OH in several low-mass YSOs, possibly indicating that the conditions required for production of CH_3OH are not limited to high-mass YSOs.

Conditions in intermediate-mass star formation regions (i.e., AFGL 989 and R CrA IRS 1) seem to give rise to the production of large amounts of CO_2 relative to other regions, close to 30% as compared to the ~17% found in most other lines of sight (Gerakines et al. 1999; Nummelin et al. 2001). The reasons for this are unknown. The profiles are consistent with significant contributions from both polar and apolar components. CO is primarily in the polar component in some sources, though others seem to have retained a significant apolar contribution, perhaps reflecting differences in temperature and hence evaporative loss of the apolar mantle. Modest amounts of CH_3OH may be expected to form in these regions, though the *ISO* data result in abundances consistent with those found for low-mass YSOs. Further study of such intermediate-mass regions is of great interest.

High-mass star formation regions can be divided into two distinct groups: those that show significant processing of the ice mantles and those that do not. Both groups have CO_2 abundances consistent with those found for low-mass and quiescent regions and are typically dominated by a polar component,

TABLE 24
S140 IRS 1 SPECTRAL FEATURES

λ (μm)	FWHM (cm^{-1})	τ	Species	N (10^{17} cm^{-2})	$N/N(H_2O)$ *100	Reference
3.0	335	1.12(0.02)	H_2O	19(0.3)	100	1
3.25	74	0.036(0.007)	C-H stretch	...	...	2
	68	0.050	PAH	9.4	...	3
3.46	89	0.048(0.01)	HAC	...	...	3, 4
3.54	30	<0.03	CH_3OH	<1.5	<7.7	4
3.95	115.3	<0.01	CH_3OH	<2.5	<13.3	4
4.27	23.9	1.25(0.04)	CO_2	4.2(0.1)	22	5
4.38	5	0.050(0.005)	$^{13}CO_2$	0.038(0.003)	0.16(0.02)	6
4.5[a]	700	[0.026]	H_2O	[19]	[100]	
4.62	28	~0.024	XCN	~0.14	~0.75	4
4.67[b]	7.64	<0.1	CO	...	...	7
4.91	23	<0.02	OCS	<0.05	<0.3	4
6.02	157	0.084(0.01)	H_2O	19(2)	100(11)	8
6.0	124	0.02(0.01)	Organic residue	...	...	8
6.85	76	0.087(0.01)	Organics/NH_4^+	...	...	8
7.243	16.8	<0.010	HCOOH	<0.69	<3.6	4
	19.8		CH_3HCO	<0.26	<1.4	4
7.414	17.8	<0.005	$HCOO^-$	<0.056	<0.29	4
	10.6		CH_3HCO	<0.38	<2.0	4
7.676	10	0.012(0.003)	CH_4	0.17(0.04)	0.92(0.2)	4
9.0	68	<0.013	NH_3	<0.68	<3.6	1
9.7	266	1.51(0.02)	Silicate	...	...	4
13.3[a]	240	[0.23]	H_2O	[19]	[100]	
15.2	16.3	0.24(0.02)	CO_2	4.2(0.1)	22	5
			(Polar)	2.1	11	5
			(Nonpolar)	2.1	11	5
18	173	0.40(0.03)	Silicate	...	...	4

[a] Calculated from 3 μm feature.
[b] Gas phase CO.

REFERENCES.—(1) Gibb et al. 2001; (2) Brooke et al. 1999; (3) Bregman & Temi 2001; (4) this work; (5) Gerakines et al. 1999; (6) Boogert et al. 2000; (7) Tielens et al. 1991; (8) Gibb & Whittet 2002.

TABLE 25
NGC 7538 IRS 1 Spectral Features

λ (μm)	FWHM (cm^{-1})	τ	Species	N (10^{17} cm^{-2})	$N/N(H_2O)$ *100	Reference
3.0	335	1.27	H_2O	22	100	1
3.25	74	0.078(0.013)	C-H stretch	...	...	2
3.29	49	...	PAH emission	...	...	3
3.39	16.6	...	HAC emission	...	...	3
3.46	80	−0.046	HAC	...	...	3
3.54	30	<0.02	CH_3OH	<1	<4	3
3.95	115.3	<0.01	CH_3OH	<2.3	<10	3
4.27	16.4	2.03(0.11)	CO_2	5.1(0.2)	23(0.9)	4
4.38	7.2	0.09	$^{13}CO_2$	0.11	0.5	3
4.5[a]	700	[0.03]	H_2O	[22]	100	3
4.62	29	<0.02	XCN	<0.1	<0.5	3
4.67	7.64	0.26	CO	1.8	8.2	3
		0.07	(Polar)	0.99	4.5	3
		0.15	(Nonpolar)	0.86	3.9	3
4.91	23	<0.01?	OCS	<0.01?	<0.05	3
6.02[a]	185	[0.08]	H_2O	[22]	[100]	3
6.0		~0.18	Organic residue?	...	...	3
6.22		...	PAH emission	...	...	
6.85	105	0.27(0.01)	Organics	...	...	3
7.273	25.4	0.046(0.007)	HCOOH	4.8(0.7)	22(3)	3
			$HCOO^-$	1.6(0.2)	7.3(1)	3
7.414	17.8	0.034(0.006)	$HCOO^-$	0.38(0.07)	1.7(0.3)	3
	10.6		CH_3HCO	2.6(0.5)	12(2)	3
7.676	10.4	0.022(0.007)	CH_4???	0.33(0.1)	1.5(.5)	3
9.0	68	<0.071	NH_3	<3.7	<17	1
9.7	307	1.98(0.06)	Silicate	...	...	3
13.3[a]	240	[0.30]	H_2O	[22]	100	3
15.2	24.3	0.21(0.01)	CO_2	5.1(0.2)	23(0.9)	4
			(Polar)	4.5	20	4
			(Nonpolar)	0.6	2.7	4
18	230	0.62(0.02)	Silicate	...	...	3

Note.—There are emission features at 2.626 μm (Brβ), 2.757 μm (Pfη), 2.872 μm (Pfζ), 3.037 μm (Pfϵ), 3.296 μm (Pfδ), 3.741 μm (Pfγ), 4.052 μm (Brα), 4.653 μm (Pfβ), 6.981 μm (Ar II $^2P_{1/2}-^2P_{3/2}$), 7.458 μm (Pfα), 8.989 μm (Ar III $^3P_1-^3P_2$), 12.808 μm (Ne II $^2P_{1/2}-^2P_{3/2}$), 18.710 μm (H I 22–12, S III $^3P_2-^3P_1$?), 33.474 μm (Si III $^3P_1-^3P_0$?), and 34.805 μm (Si II $^2P_{3/2}-^2P_{1/2}$?).

[a] Calculated from the 3 μm feature.

References.—(1) Gibb et al. 2001; (2) Brooke et al. 1999; (3) this work; (4) Gerakines et al. 1999.

though a significant apolar component is suggested by the profiles of many of these objects. CO in these regions is primarily in the gas phase, though many sources have retained a significant CO mantle with both polar and apolar components, probably originating in the cool envelope surrounding the YSO. The weakly processed objects are similar to lower mass YSOs in their NH_3 and CH_3OH abundances, though processing has given rise to detectable 4.62 μm XCN features in several of these objects. Intensive processing, as for the regions W33 A, AFGL 7009S, and NGC 7538 IRS 9, leads to large abundances of CH_3OH (~15% or more) and the formation of significant (2%–6%) abundances of XCN. Large abundances of NH_3 (~15%) may also be present along these lines of sight.

5.3.1. *Carbon and Nitrogen Ice Component*

In general, the principle carbon-bearing species in the polar mantle in all lines of sight is CO_2 with the possible exceptions of those sources (W33 A and AFGL 7009S) with high methanol abundances. The total contribution of polar CO and CO_2 is typically 10%–30% that of the dominant component, water, though for the high CO_2, intermediate-mass YSOs (such as R CrA IRS 1) the percentage can be as high as 40%. For most sources in this study, these are the only carbon-bearing species for which firm abundances are known. Other carbon-bearing ices (CH_3OH, HCOOH, CH_4, and H_2CO) may contribute no more than ~10% in most lines of sight. The exceptions to this are the strongly processed massive YSOs for which $CH_3OH+CH_4+HCOOH+H_2CO$ may contribute up to an additional 20%, bringing the total contribution of carbon-bearing ices in the polar mantle to nearly half that of water. The apolar mantle varies strongly, depending critically on the temperature profile through the line of sight.

Nitrogen, on the other hand, is apparently far less abundant on the grain surface. In most lines of sight, the total possible contribution from ammonia and XCN is less than 10% and frequently less than 5%. The only exceptions to this are the strongly processed massive YSOs for which NH_3+XCN could contribute as much as 15%–20% relative to water. Presumably, most of the nitrogen in the ices is in the form of N_2, which lacks infrared signatures.

5.3.2. *Implications for Grain Surface Chemistry*

Keane (2002) investigated grain surface chemistry in interstellar clouds. In particular, it was determined from five high-mass YSOs that the high abundance of solid H_2O and the

TABLE 26
NGC 7538 IRS 9 Spectral Features

λ (μm)	FWHM (cm^{-1})	τ	Species	N (10^{17} cm^{-2})	$N/N(H_2O)$ *100	Reference
3.0	439	3.1(0.25)	H_2O	70(6)	100	1, 2
3.485	98.8	0.130(0.017)	HAC	...	...	3
3.54	29	0.07(0.01)	CH_3OH	3.0(0.4)	4.3(0.6)	3
3.95	115.3	<0.012	CH_3OH	<2.9	<4.2	1
4.27	20	>5	CO_2	16.3(1.8)	23.3(2.6)	4
4.38	10.4	0.15(0.01)	$^{13}CO_2$	0.203(0.012)	0.290(0.017)	5
4.5[a]	700	[0.094]	H_2O	[70]	[100]	1
4.62	20	0.21	XCN	1.2	1.7	6, 7
4.67	4.75	2.6(0.2)	CO	12(1)	17(1)	8
		0.2(0.1)	(Polar)	1.4(0.8)	2.0(1.1)	8
		2.5(0.2)	(Nonpolar)	11(1)	16(1)	8
4.91	17.6	0.05(0.01)	OCS	0.055(0.044)	0.079(0.063)	1
5.83	30	0.06(0.02)	H_2CO	1.5(0.5)	2.2(0.7)	9
5.85	65	0.05(0.02)	HCOOH	0.69(0.28)	0.98(0.40)	9
6.02[a]	158	0.31(0.02)	H_2O	70(4.5)	100(6.4)	9
6.0		0.18(0.02)	Organic residue	...	...	9
6.85	83	0.34(0.02)	Organics/NH_4^+	...	...	9
7.243	16.8	<0.016	HCOOH	<1.1	<1.6	1
	19.8		CH_3HCO	<0.42	<0.60	1
7.414	17.8	<0.016	$HCOO^-$	<0.18	<0.26	1
	10.6		CH_3HCO	<1.2	<1.7	1
7.58	27.7	<0.06	SO_2	<0.55	<0.79	10
7.674	10.7	0.092(0.005)	CH_4	1.05(0.03)	1.5(0.04)	11
8.90[a]	34	[0.011]	CH_3OH	[$\sim$3.0]	[$\sim$4.3]	1
9.0	68	0.20(0.04)	NH_3	10.5(1.9)	15(2.7)	12
9.7	242	2.23	Silicate	...	...	1
9.75[a]	30	[0.18]	CH_3OH	[3.0]	[4.3]	1
13.3[a]	240	[0.63]	H_2O	[70]	[100]	1
15.2	21.1	0.766(0.005)	CO_2	16.3(1.8)	23.3(2.6)	4
			(Polar)	10.8	15.4	4
			(Nonpolar)	5.5	7.9	4
18	217	0.56	Silicate	...	...	1

[a] Water values calculated from 3 μm feature and CH_3OH values from the 3.54 μm feature.

References.—(1) This work; (2) Allamandola et al. 1992; (3) Brooke et al. 1999; (4) Gerakines et al. 1999; (5) Boogert et al. 2000; (6) Whittet et al. 2001; (7) Demyk et al. 1998; (8) Chiar et al. 1998; (9) Gibb & Whittet 2002; (10) Boogert et al. 1997; (11) Boogert et al. 1996; (12) Gibb et al. 2001.

CO_2:CO and CH_3OH:CO ratios imply that both oxygenation and hydrogenation reactions are important for determining ice mantle compositions. Our results are consistent with this interpretation. The CO_2:CO ratio is found to range from about 1–4 in all our sources, including quiescent and low/intermediate-mass regions. CH_3OH:CO is found to range from 0.11 or less to $\sim$1. When compared with the model of Keane (2002) we deduce that the observed ice mantle composition in a wide range of physical environments requires a high O_2 abundance, a conclusion reached by Keane (2002) for high-mass YSOs alone.

6. CONCLUSION

Our understanding of interstellar ices has clearly come a long way since the launch of the pivotal *Infrared Space Observatory*. While H_2O, CO, CO_2, CH_3OH, and CH_4 seem to be well characterized in many lines of sight, there are still many mysteries regarding the nitrogen component of the grain mantle. Such features as the 4.62 μm XCN and 6.8 μm organic/NH_4^+ are thought to originate primarily via processing of NH_3-bearing ices, yet there is much controversy and contradiction in the literature concerning the abundance of ammonia in ices. The water-ice features at 3 and 6 μm contain structure and/or blended features that are still not fully understood. Clearly, much more work needs to be done to characterize ice composition in a variety of lines of sight, from the diffuse ISM to quiescent clouds and through the range of star formation environments. While many advances are being accomplished with the use of ground-based instrumentation (i.e., Dartois et al. 2002; Boogert et al. 2002; Taban et al. 2003; Pontoppidan et al. 2003), another space-based mission with high resolving power (>2000) and greater sensitivity to improve studies of low-mass and quiescent environments is needed to fully understand the volatile component of the interstellar medium.

E. L. G. and D. C. B. W. gratefully acknowledge financial support from NASA under grants NAG5-7598 and NAG5-9148. E. L. G. also gratefully acknowledges support from the National Research Council under her Resident Research Associateship. The data presented were analyzed with the support of the Dutch *ISO* Data Analysis Centre (DIDAC) at the Space Research Organization Netherlands (SRON) in Groningen, the Netherlands.

TABLE 27

Ice Composition as a Function of Environment

Source Type	H_2O	CO_2	CO	NH_3	CH_3OH	XCN	6.0 μm Excess	Sources
Quiescent environment	100	~25	~25	<10	<3	<1.5	...	Elias 16
Low-mass YSO	100	~20	~5	<5	<5	<0.2	Intermediate	Elias 29
Intermediate-mass YSO	100	~30–35	18–50	<5	<5	~0.3	Intermediate	AFGL 989, R CrA IRS 1, R CrA IRS 2
High-mass YSO, weak processing	100	~7–22	~3–8	<5	<5–10	0.3–2	Weak to strong	W3 IRS 5, AFGL 490, Orion BN, Orion IrC2, Mon R2 IRS 2, Mon R2 IRS 3, AFGL 2136, AFGL 2591, S140, NGC 7538 IRS 1, NGC 7538 IRS 9
High-mass YSO, strong processing	100	~13–23	8–17	~15	~15–30	2–6	Strong	W33A, AFGL 7009S

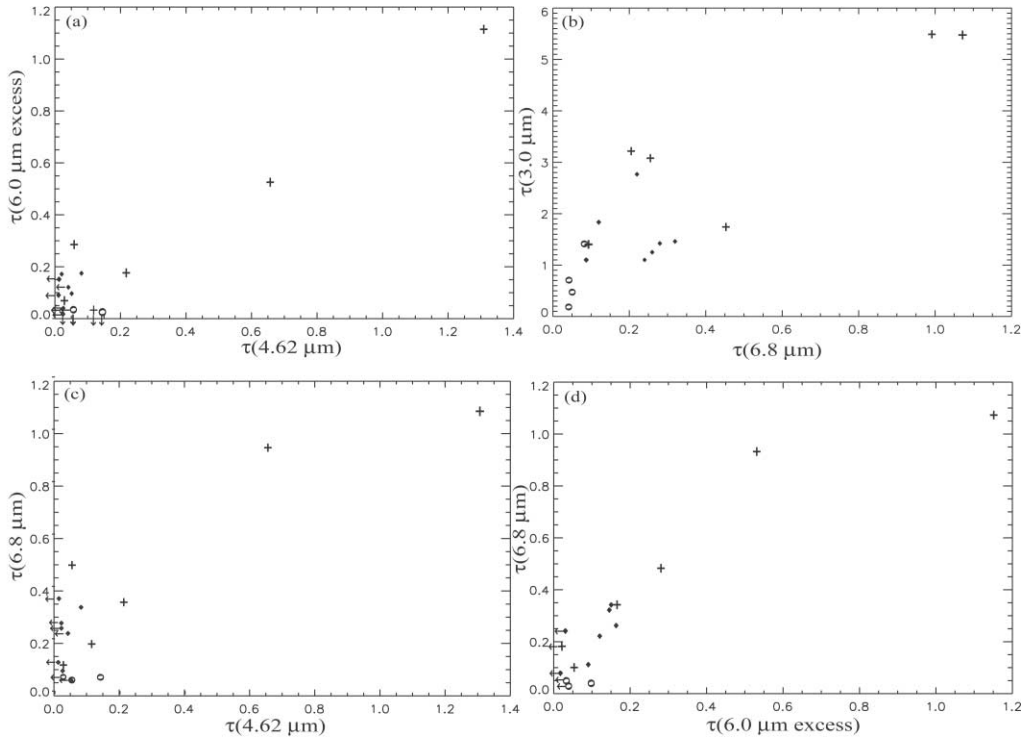

FIG. 2.—Correlation plots showing the peak optical depths of (*a*) the excess absorption at 6.0 μm vs. XCN, (*b*) the 3.0 μm H_2O feature vs. the 6.8 μm feature, (*c*) the 6.8 μm feature vs. XCN, and (*d*) the 6.8 μm feature vs. the excess at 6.0 μm. The excess at 6.0 μm was determined by subtracting the water contribution as determined from the 3.0 μm feature. The 6.8 μm optical depth was determined after subtraction of known contributions due to H_2O and CH_3OH. The diamonds are sources for which the 6.8 μm feature peaks at higher wavelength, while the plus signs represent sources with substantial contributions from both components in Keane et al. (2001c). The circles are sources for which the 6.8 μm feature is weak and noisy.

REFERENCES

Aitken, D. K., Smith, C. H., James, S. D., Roche, P. F., & Hough, J. H. 1988, MNRAS, 230, 629
Allamandola, L. J., Sandford, S. A., Tielens, A. G. G. M., & Herbst, T. M. 1992, ApJ, 399, 134
Allamandola, L. J., Sandford, S. A., & Valero, G. J. 1988, Icarus, 76, 225
Allen, D. A. 1972, ApJ, 172, L55
Bernstein, M. P., Dworkin, J. P., Sandford, S. A., Cooper, G. W., & Allamandola, L. J. 2002, Nature, 416, 401
Bernstein, M. P., Sandford, S. A., Allamandola, L. J., Chang, S., & Scharberg, M. A. 1995, ApJ, 454, 327
Bockelée-Morvan, D., et al. 2000, A&A, 353, 1101
Boogert, A. C. A., Blake, G. A., & Tielens, A. G. G. M. 2002, ApJ, 577, 271
Boogert, A. C. A., Helmich, F. P., van Dishoeck, E. F., Schutte, W. A., Tielens, A. G. G. M., & Whittet, D. C. B. 1998, A&A, 336, 352
Boogert, A. C. A., Schutte, W. A., Helmich, F. P., Tielens, A. G. G. M., & Wooden, D. H. 1997, A&A, 317, 929
Boogert, A. C. A., et al. 1996, A&A, 315, L377
———. 2000, A&A, 353, 349
Boonman, A. M. S., van Dishoeck, E. F., Lahuis, F., Wright, C. M., & Doty, S. D. 2003, A&A, 399, 1063
Bowey, J. E., Adamson, A. J., & Whittet, D. C. B. 1998, MNRAS, 298, 131
Bregman, J. D., Hayward, T. L., & Sloan, G. C. 2000, ApJ, 544, L75
Bregman, J. D., & Temi, P. 2001, ApJ, 554, 126
Brooke, T. Y., Sellgren, K., & Geballe, T. R. 1999, ApJ, 517, 883
Brooke, T. Y., Sellgren, K., & Smith, R. G. 1996, ApJ, 459, 209
Capps, R. W., Gillett, F. C., & Knacke, R. F. 1978, ApJ, 226, 863
Carr, J. S., Evans II, N. J., Lacy, J. H., & Zhou, S. 1995, ApJ, 450, 667
Chen, H., Myers, P. C., Ladd, E. F., & Wood, D. O. S. 1995, ApJ, 445, 377
Chiar, J. E., Adamson, A. J., Kerr, T. H., & Whittet, D. C. B. 1994, ApJ, 426, 240
———. 1995, ApJ, 455, 234
Chiar, J. E., Adamson, A. J., Pendleton, Y. J., Whittet, D. C. B., Caldwell, D. A., & Gibb, E. L. 2002, ApJ, 570, 198
Chiar, J. E., Adamson, A. J., & Whittet, D. C. B. 1996, ApJ, 472, 665
Chiar, J. E., Gerakines, P. A., Whittet, D. C. B., Pendleton, Y. J., Tielens, A. G. G. M., Adamson, A. J., & Boogert, A. C. A. 1998, ApJ, 498, 716
Chiar, J. E., Tielens, A. G. G. M., Whittet, D. C. B., Schutte, W. A., Boogert, A. C. A., Lutz, D., van Dishoeck, E. F., & Bernstein, M. P. 2000, ApJ, 537, 749
Choi, M., Evans II, N. J., Tafalla, M., & Bachiller, R. 2000, ApJ, 538, 738
Cronin, J. R., & Pizzarello, S. 1990, Geochim. Cosmochim. Acta, 54, 2859
Dartois, E., & d'Hendecourt, L. 2001, A&A, 365, 144
Dartois, E., d'Hendecourt, L., Thi, W., Pontoppidan, K. M., & van Dishoeck, E. F. 2002, A&A, 394, 1057
Dartois, E., Schutte, W., Geballe, T. R., Demyk, K., Ehrenfreund, P., & d'Hendecourt, L. 1999, A&A, 342, L32
Dartois, E., et al. 1998, A&A, 338, L21
de Graauw, Th., et al. 1996, A&A, 315, L49
de Muizon, M. J., d'Hendecourt, L., & Geballe, T. R. 1990, A&A, 235, 367
Demyk, K., Dartois, E., d'Hendecourt, L., Jourdain de Muizon, M., Heras, A. M., & Breitfellner, M. 1998, A&A, 339, 553
d'Hendecourt, L., & Allamandola, L. J. 1986, A&AS, 64, 453
d'Hendecourt, L., & Jourdain de Muizon, M. 1989, A&A, 223, L5
d'Hendecourt, L., et al. 1996, A&A, 315, L365
Ehrenfreund, P., Bernstein, M. P., Dworkin, J. P., Sandford, S. A., & Allamandola, L. J. 2001, ApJ, 550, L95
Elias, J. H. 1978, ApJ, 224, 857
Evans, N. J., Mundy, L. G., Kutner, M. L., & Depoy, D. L. 1989, ApJ, 346, 212
Georgelin, Y. M., & Georgelin, Y. P. 1976, A&A, 49, 57
Gerakines, P. A., Schutte, W. A., Greenbert, J. M., & van Dishoeck, E. F. 1995, A&A, 296, 810
Gerakines, P. A., et al. 1999, ApJ, 522, 357
Gezari, D. Y., Backman, D. E., & Werner, M. W. 1998, ApJ, 509, 283
Gibb, E. L., & Whittet, D. C. B. 2002, ApJ, 566, 113
Gibb, E. L., Whittet, D. C. B., & Chiar, J. E. 2001, ApJ, 558, 702
Gibb, E. L., et al. 2000, ApJ, 536, 347
Goss, W. M., Matthews, H. E., & Winneberg, A. 1978, A&A, 65, 307
Greenberg, J. M., Li, A., Mendoza-Gomez, C. X., Schutte, W. A., Gerakines, P. A., & de Groot, M. 1995, ApJ, 455, L177
Grishko, V. I., & Duley, W. W. 2000, ApJ, 543, L85
Gürtler, J., Klaas, U., Henning, Th., Ábrahám, P., Lemke, D., Schreyer, K., & Lehmann, K. 2002, A&A, 390, 1075
Hanner, M. S., Brooke, T. Y., & Tokunaga, A. T. 1994, ApJ, 433, L97

Henning, Th., Pfau, W., & Altenhoff, W. J. 1990, A&A, 227, 542
Hiraoka, K., Sato, T., Sato, S., Sogoshi, N., Yokoyama, T., Hideaki, T., & Kitagawa, S. 2002, ApJ, 577, 265
Hudgins, D. M., Sandford, S. A., Allamandola, L. J., & Tielens, A. G. G. M. 1993, ApJS, 86, 713
Hudson, R. L., & Moore, M. H. 1995, Radiat. Phys. Chem., 45, 779
Hudson, R. L., Moore, M. H., & Gerakines, P. A. 2001, ApJ, 550, 1140
Humphreys, R. M. 1978, ApJS, 38, 309
Keane, J. V. 2002, Ph.D. thesis, Univ. Groningen
Keane, J. V., Boogert, A. C. A., Tielens, A. G. G. M., Ehrenfreund, P., & Schutte, W. A. 2001a, A&A, 375, L43
Keane, J. V., Boonman, A. M. S., Tielens, A. G. G. M., & van Dishoeck, E. F. 2001b, A&A, 376, L5
Keane, J. V., Tielens, A. G. G. M., Boogert, A. C. A., Schutte, W. A., & Whittet, D. C. B. 2001c, A&A, 376, 254
Kerkhof, O., Schutte, W. A., & Ehrenfreund, P. 1999, A&A, 349, 990
Koresko, C. D., Beckwith, S., Ghez, A. M., Matthews, K., Herbst, T. M., & Smith, D. A. 1993, AJ, 105, 1481
Lacy, J. H., Farah, H., Sandford, S. A., & Allamandola, L. J. 1998, ApJ, 501, L105
Ladd, E. F., Deane, J. R., Sanders, D. B., & Wynn-Williams, C. G. 1993, ApJ, 419, 186
Lahuis, F., & van Dishoeck, E. F. 2000, A&A, 355, 699
Lutz, D., et al. 1996, A&A, 315, L269
Marraco, H. G., & Rydgren, A. E. 1981, AJ, 86, 62
Minchin, N. R., Hough, J. H., Burton, M. G., & Yamashita, T. 1991, MNRAS, 251, 522
Mitchell, G. F., Allen, M., & Maillard, J.-P. 1988, ApJ, 333, L55
Mitchell, G. F., & Hasegawa, T. I. 1991, ApJ, 371, L33
Mitchell, G. F., Lee, S. W., Maillard, J. P., Matthews, H., Hasegawa, T. I., & Harris, A. I. 1995, ApJ, 438, 794
Mitchell, G. F., Maillard, J. P., Allen, M., Beer, R., & Belcourt, K. 1990, ApJ, 363, 554
Moneti, A., Cernicharo, J., & Pardo, J. R. 2001, ApJ, 549, L203
Mozurkewich, D., Schwartz, P. R., & Smith, H. A. 1986, ApJ, 311, 371
Munoz Caro, G. M., et al. 2002, Nature, 416, 403
Nummelin, A., Whittet, D. C. B., Gibb, E. L., Gerakines, P. A., & Chiar, J. E. 2001, ApJ, 558, 185
Palumbo, M. E., Geballe, T. R., & Tielens, A. G. G. M. 1997, ApJ, 479, 839
Pendleton, Y. J., Tielens, A. G. G. M., Tokunaga, A. T., & Bernstein, M. P. 1999, ApJ, 513, 294
Pontoppidan, K. M., Dartois, E., van Dishoeck, E. F., Thi, W.-F., & d'Hendecourt, L. 2003, A&A, 404, L17
Rieke, G. H., & Lebofsky, M. J. 1985, ApJ, 288, 618
Salama, F., Allamandola, L. J., Witteborn, F. C., Cruikshank, D. P., Sandford, S. A., & Bregman, J. D. 1990, Icarus, 83, 66
Sandford, S. A., & Allamandola, L. J. 1990, Icarus, 87, 188
Sandford, S. A., Allamandola, L. J., Tielens, A. G. G. M., & Valero, L. J. 1988, ApJ, 329, 498
Schreyer, K., Helmich, F. P., van Dishoeck, E. F., & Henning, Th. 1997, A&A, 326, 347
Schutte, W. A., Allamandola, L. J., & Sandford, S. A. 1993, Icarus, 104, 118
Schutte, W. A., Gerakines, P. A., Geballe, T. R., van Dishoeck, E. F., & Greenberg, J. M. 1996, A&A, 309, 633
Schutte, W. A., & Greenberg, J. M. 1997, A&A, 317, L43
Schutte, W. A., & Khanna, R. K. 2003, A&A, 398, 1049
Schutte, W. A., et al. 1998, A&A, 337, 261
———. 1999, A&A, 343, 966
Sellgren, K., Smith, R. G., & Brooke, T. Y. 1994, ApJ, 433, 179
Skinner, C. J., Tielens, A. G. G. M., Barlow, M. J., & Justtanont, K. 1992, ApJ, 399, L79
Smith, R. G., Sellgren, K., & Tokunaga, A. T. 1989, ApJ, 344, 413
Smits, D. P., Cohen, R. J., & Hutawaradorn, B. 1998, MNRAS, 296, L11
Snell, R. L., Scoville, N. Z., Sanders, D. B., & Erickson, N. R. 1984, ApJ, 284, 176
Snyder, L. E. 1997, Origins Life Evol. Biosphere, 27, 115
Strazzulla, G., Nisini, B., Leto, G., Paulumbo, M. E., & Saraceno, P. 1998, A&A, 334, 1056
Taban, I. M., Schutte, W. A., Pontoppidan, K. M., & van Dishoeck, E. F. 2003, A&A, 399, 169
Teixeira, T. C., & Emerson, J. P. 1999, A&A, 351, 303
Thompson, R. I., Corbin, M. R., Young, E., & Schneider, G. 1998, ApJ, 492, L177
Tieftrunk, A. R., Gaume, R. A., Claussen, M. J., Wilson, T. L., & Johnston, K. J. 1997, A&A, 318, 931
Tielens, A. G. G. M., & Hagen, W. 1982, A&A, 114, 245
Tielens, A. G. G. M., Meixner, M. M., van der Werf, P. P., Bregman, J., & Tauber, J. A. 1993, Science, 262, 86
Tielens, A. G. G. M., Tokunaga, A. T., Geballe, T. R., & Baas, F. 1991, ApJ, 381, 181
Torres-Dodgen, A. V., Tapia, M., & Carroll, M. 1991, MNRAS, 249, 1
van der Tak, F. S., van Dishoeck, E. F., Evans II, N. J., & Blake, G. A. 1999, ApJ, 522, 991
van Dishoeck, E. F., Wright, C. M., Cernicharo, J., Gonzalez-Alfonso, E., de Graauw, Th., Helmich, F. P., & Vandenbussche, B. 1998, ApJ, 502, L173
Watanabe, N., & Kouchi, A. 2002, ApJ, 571, L173
Werner, M. W., Becklin, E. E., Gatley, I., Matthews, K., & Neugebauer, G. 1979, MNRAS, 188, 463
Whittet, D. C. B. 2003, Dust in the Galactic Environment (Bristol: Inst. Phys. Publ.)
Whittet, D. C. B., Bode, M. F., Longmore, A. J., Baines, D. W. T., & Evans, A. 1983, Nature, 303, 218
Whittet, D. C. B., Pendleton, Y. J., Gibb, E. L., Boogert, A. C. A., Chiar, J. E., & Nummelin, A. 2001, ApJ, 550, 793
Whittet, D. C. B., et al. 1996, ApJ, 458, 363
———. 1997, ApJ, 490, 729
———. 1998, ApJ, 498, L159
Wilking, B. A., Taylor, K. N. R., & Storey, J. W. V. 1986, AJ, 92, 103
Willner, S. P., et al. 1982, ApJ, 253, 174
Woon, D. E. 2002, ApJ, 571, L177
Wynn-Williams, C. G. 1982, ARA&A, 20, 587